Field Studies on Response of a Floating Sea Ice Sheet to a Steadily Moving Load*

by

Takatoshi TAKIZAWA
滝 沢 隆 俊
The Institute of Low Temperature Science

Received December 1987

Abstract

The results of a field experiment are presented and discussed. A skidoo was used as a moving load, and the test speed ranged from 0 to 14.2 m/s. The thickness of the ice sheet was 0.17−0.18 m, the ice temperature was −2.5 to −4.0°C at the surface, and the water depth was 6.8 m. The experimental results indicate the existence of a critical speed u_c, at which the ice deflection is amplified markedly, and its value is estimated to be 5.8 m/s. At speeds above this value, two ice waves are generated, one ahead of and the other behind the load. At u_c the depression around the load is maximal in depth and minimal in width. The center of the depression begins to lag behind the load at fairly low speeds below u_c. Using the dispersion relation for flexural free waves in a floating ice sheet, a diagram that predicts the critical speed is presented. An understanding of the group velocity provides one explanation for the question of why two waves appear in front of and at the rear of the load. The two-dimensional deflection patterns obtained in the experiment are shown and compared with the existing theoretical results. At high speeds, the ice beneath the load is found to be not depressed but to be somewhat elevated. Results also show that viscous damping has substantial effects on the ice deflection profile. The wavenumber curves, which give the two-dimensional wave patterns, are studied, and the results verify that the one-dimensional model is appropriate to discuss the wave characteristics in the present experiment. Finally, the ice response is classified into five stages.

* Contribution No. 3119 from the Institute of Low Temperature Science.
北海道大学審査学位論文

Contents

I. Introduction

The life-style and communications in cold regions are often impaired by snow and ice in winter. However, there are many positive aspects of the winter cold. Easy construction of aircraft runways and winter roads on floating ice sheets (namely, sea ice, river ice and so on) is a typical example. Such facilities provide greater transportation convenience than those used in the summer. In recent years, the increase of human activities in the polar regions, such as oil developments in the Arctic, has prompted the need for more extensive use of the ice sheets for various purposes. However, to ensure safety and appropriate usage, more information on the load bearing capacity of ice covers is required. As for static loads, many investigations have been made and a wide knowledge has been accumulated. A comprehensive review has been given by Kerr (1976).

One of the most important subjects dealing with moving loads is the dynamic response of ice sheets to them. When the vehicle speed and the ice thickness have specific values, it is possible for an ice deflection under a moving vehicle to become amplified markedly and for ice waves to develop simultaneously. This possibility, in which the specific vehicle speed is defined as the critical speed u_c, has been suggested and treated theoretically by Wilson (1958) and Nevel (1970), while its phenomena have been observed in field experiments (Wilson, 1958 ; Eyre and Hesterman, 1976 ; Eyre, 1977 ; Takizawa, 1978 ; Beltaos, 1979).

Wilson (1958) proposed a theory for predicting the generation of two different ice waves, one ahead of the load (leading wave) and the other behind it (trailing wave). On the basis of the experimental results, however, Eyre and Hesterman (1976) and Eyre (1977) concluded that the moving load generated only one orderly wave in front of it. Furthermore, Beltaos (1979) observed the leading wave alone. Meanwhile, Takizawa (1978) found that two waves were generated, though the trailing wave disappeared at a speed not much greater than u_c. The ice wave is one of the substantial reactions of the floating ice sheet to the moving load, but the question of whether the moving load generates one wave or two waves remains unsolved.

Another noticeable feature of the ice response is the lag of the maximum deflection position behind the load. The previous experiments (Eyre, 1977 ; Takizawa, 1978 ; Beltaos, 1979) showed the different results in the speed when the lag arose. The lag took place at $u \sim 0.85u_c$ (Eyre), $u \sim 0.9u_c$ (Takizawa), or $u \sim 1.2u_c$ (Beltaos). At present, like these different results show, the lag of the maximum deflection position is poorly understood.

Squire *et al.* (1985) measured the strains in ice sheets due to a moving vehicle. The experimental results were discussed in the context of theoretical works derived from existing solutions. Davys *et al.* (1985) solved an equation of the motion of an ice sheet subjected to a steadily moving load using asymptotic Fourier analysis to give a description of the wave patterns far away from the load. Their solution elucidated the spatial nature of the wave

field. They also conducted some experiments and compared the obtained wave records with theoretical predictions. Schulkes *et al.* (1986) extended the work of Davys *et al.* (1985) and discussed the effects of in-plane forces and of uniform flow and stratification in the underlying water on ice wave characteristics. Furthermore, Schulkes and Sneyd (1986) studied the effect of an impulsively applied concentrated line load moving with uniform speed and investigated the time-dependent effects.

The purpose of the present study is to analyse the results of an extensive field experiment which was conducted to clarify the characteristics of ice deflection patterns, and to reach a more accurate understanding of the response nature of a floating ice sheet to a steadily moving load. Section II describes the experimental site and procedure. The experimental results are given in Section III. Generally, it is difficult to solve analytically an equation of motion for an ice sheet subjected to a moving load. Thus, Section IV describes the dispersion relation for the ice waves induced by a moving load and the critical speed, using the dispersion relation for flexural free waves in a floating ice sheet. In Section V, spatial characteristics of the deflection patterns are presented. Comparison is then made with the theoretical prediction of Davys *et al.* (1985). Section VI describes the viscous damping effects. The ice response is classified into five stages in Section VII. In Section VIII, several significant properties of ice deflections are discussed.

II. Experimental site and instrumentation

The experiment was carried out from February 4—10, 1981, at Lake Saroma (44°10' N, 143°50' E) in Hokkaido, Japan (Fig. 1). The lake is a large elliptical lagoon with a northwest-southeast length of about 26 km and a northeast-southwest width of about 12 km. The basin is saucer-shaped, with a maximum water depth of 19.6 m.

Table 1 Experimental conditions

Ice thickness, h	0.17 — 0.18 m
Snow cover	0.02 — 0.08 m
Water depth, H	6.8 m
Air temperature	−2.0 — −11.0 °C
Ice temp. (surface)	−2.5 — −4.0 °C
(0.05 m)	−2.3 — −3.3 °C
(0.10 m)	−2.4 — −3.3 °C
(0.15 m)	−2.0 — −2.4 °C
Water temperature	−1.8 °C

The lake began to freeze at the end of January. The formed sea ice (7.7 ‰ in salinity) was very flat at its surface, on which a test track of 400 m in length was prepared parallel to the shoreline at a distance of about 1 km from the shore. The experimental conditions are listed in Table 1. The ice thickness was measured daily at three randomly selected points along the track, and the mean value was calculated. Five L-tube glass thermometers were placed at depths of 0, 0.05, 0.1, 0.15 and 0.3 m from the ice surface, the upper four for the ice temperatures and the lowest for the water temperature. Another glass thermometer was used to measure air temperature. They gave the temperatures in

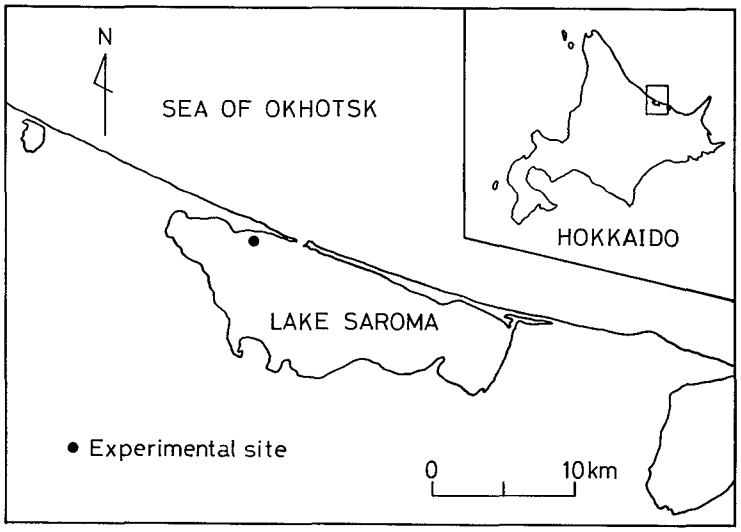

Fig. 1 Location of the experimental site.

the daytime during the experimental period. The air temperature dropped exceptionally to −18.6 °C on the evening of February 6.

A skidoo (2.43 m in length, 0.79 m in width, 235 kg in weight including a driver) was used as a moving load ; in addition, another skidoo (2.46 m in length, 0.935 m in width, 240 kg in weight) was used on the 8th of February.

The ice deflection was measured with three deflectometers. These were potentiometric displacement transducers that were anchored to the lake bed by thin cables (Fig. 2), and each was installed at an interval of 2 m midway between both ends of the track. They were aligned either parallel (D_1, D_2, D_3 in Fig. 3) or normal (D_1', D_2, D_3') to the direction of the track. The former set-up was called "along-track arrangement" and the latter "off-track arrangement".

To determine the location of the skidoo,

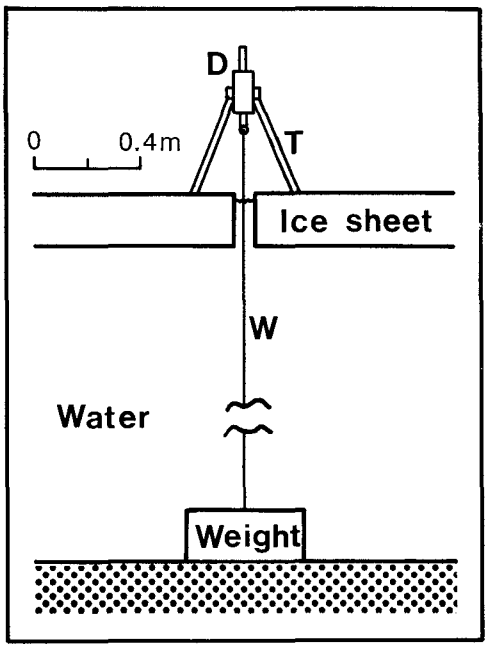

Fig. 2 Schematic diagram of the bottom-anchored deflectometer. D : Displacement transducer, T : Tripod, W : Thin cable.

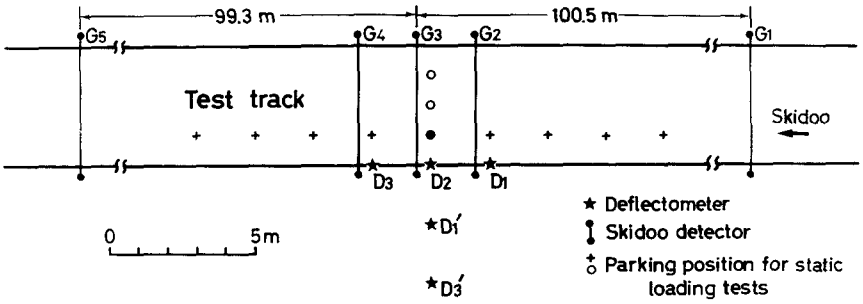

Fig. 3 Plan of the test track.

vehicle detectors were set at five points along the track as shown in Fig. 3 (G_1-G_5). The detector was a thin copper wire stretched across the track (Fig. 4). When a running skidoo broke the wire, the microswitch connected to the wire generated a pulse signal. Three detectors (G_2-G_4) were placed close to the deflectometers in such a manner that the detector worked the moment the center of the skidoo passed the deflectometer.

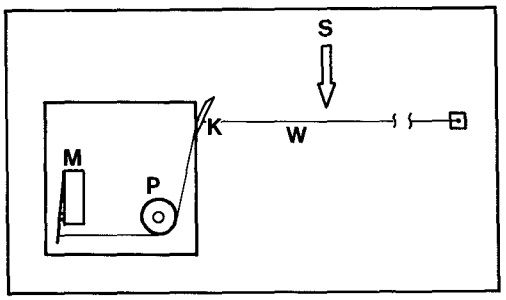

Fig. 4 Arrangement of the skidoo detector.
M : Microswitch, P : Pulley,
K : Knife edge, W : Copper wire,
S : Skidoo.

The distance between the deflectometer and the center line of the skidoo's trace was mostly 1 m for the "along-track arrangement", although some test runs were made at distances of 2 m and 3 m. For the "off-track arrangement", test runs were carried out at distances between the center line of the skidoo's trace and the nearest deflectometer D_2 of 1 m, 2 m and 3 m.

The number of test runs totaled 141, and the test speed ranged from 0 to 14.2 m/s. On each dynamic test run, the skidoo was quickly accelerated to the required speed before reaching the first skidoo detector. The speed at which the skidoo was driven through the track was kept as constant as possible thereafter. The mean speed was calculated for each test run at the interval of 199.8 m between G_1 and G_5, and this speed was adopted as the test speed.

Static loading tests were included in dynamic test sequences. In the case of the "along-track arrangement", the nine parking positions along the track were marked at an interval of 2 m, as shown in Fig. 3. The skidoo moved slowly and stopped at each parking position for about half a minute successively, from the second to the eighth position on the 5th of February, and from the first to the ninth on the 6th. In the case of the "off-track

arrangement", the skidoo was parked at distances of 1, 2 and 3 m from the nearest deflectometer, D_2, perpendicular to the direction of the track (see Fig.3). These two arrangements gave a longitudinal and a transversal profile of ice deflection in the static loading tests.

III. Experimental results

III. 1 *Static loading tests*

In the case of the "along-track arrangement", when the skidoo was parked at the j-th position, the deflection of the i-th deflectometer $\delta_i(j)$ was regarded approximately as the deflection at a distance of $2[(i+3)-j]$ m from the load, where $i=1-3$ and $j=1-9$. The obtained deflections, rearranged in accordance with the distance from the load, yielded a longitudinal profile, as shown in Fig.5a. Meanwhile, tests for the "off-track arrangement" with the similar procedure provided a transversal profile, as shown in Fig.5b.

In the longitudinal profile, the positive and negative signs of the abscissa indicate that the distance is forward and backward with respect to the skidoo, respectively. It is noticeable that the obtained profile lacked symmetry, i.e., the backward slope was steeper than the forward slope and the backward rim was considerably elevated. This asymmetry is believed to be the result from an inhomogeneous weight distribution of the skidoo ; the rear of the skidoo was heavier than the front. On the other hand, the transversal profile can be regarded as symmetrical, since the load distribution was symmetrical transversally.

Assuming that an ice plate is homogeneous, isotropic and elastic, and that it rests on an elastic foundation of the Winkler type, Hertz (1884) showed for the first time a theoretical curve for the deflection profile with a static load. Later, the same result was given by the South Manchurian Railway Company (1941), Wyman (1950) and Kubo (1958a,b). For a concentrated load, Wyman predicted the deflection δ at the radial distance r from the load by the following equation,

$$\delta(r)=\frac{P}{2\pi\rho_w L^2}\mathrm{Kei}(r/L), \tag{1}$$

where P is the mass of the load, ρ_w the water density and "Kei" Kelvin's Bessel function. The symbol L has a dimension of length, and is called the characteristic length or action radius and is defined by

$$L=\left[\frac{Eh^3}{12\rho_w g(1-\sigma^2)}\right]^{1/4}, \tag{2}$$

where E and σ are the elastic modulus and Poisson's ratio for the ice, respectively, h the ice thickness and g the acceleration due to gravity.

Substituting the test data into eq. (1), we have simultaneous equations in which only L

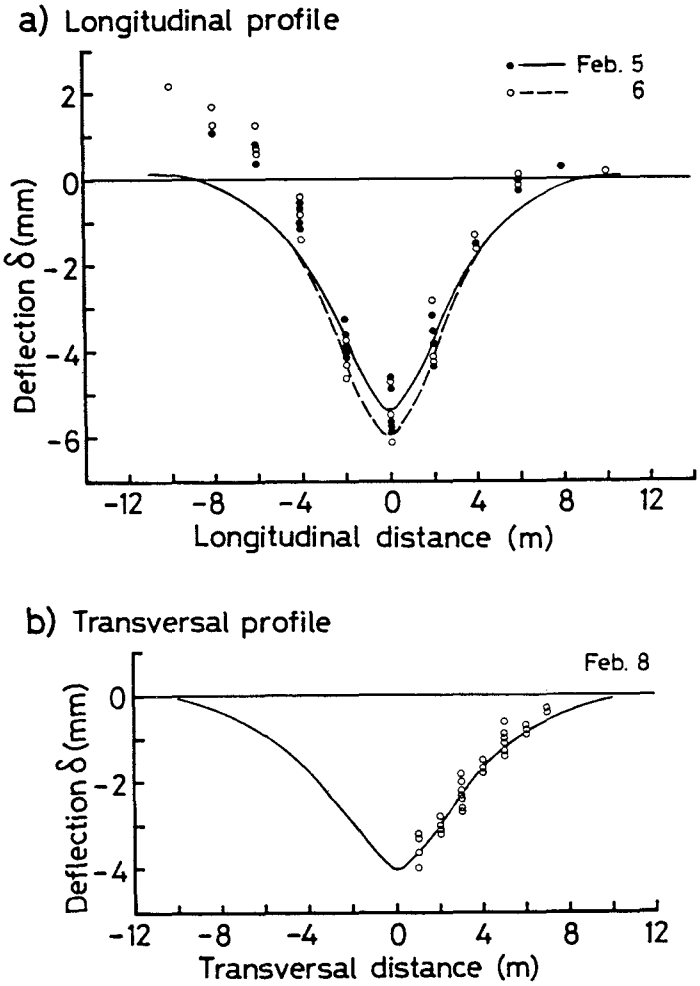

Fig. 5 Deflection profiles with static loading tests.

is unknown. Assuming that L did not vary significantly during a daily test sequence, the best-fit L in the least-squares sense was calculated for all the daily data with $g=9.8$ m/s^2 and $\rho_w=1026$ kg/m^3. Since the profile data given in Fig. 5a were not symmetrical for the longitudinal profile, the calculation was made using only the half-side data (ahead of the skidoo) ; moreover, the points of $r=0$ were omitted, because the deflections of $r=0$ were practically measured at the transversal distance of 1 m. Resultant values of L for each test data set are given in Table 2. Theoretical curves based on the values of L are plotted in Fig. 5. The curves are in good agreement with the data points, except for the backward

data, which were not taken into account for in the derived values of L.

The obtained L values enabled us to calculate the corresponding values for E through eq. (2) with an assumption of constant σ. Assuming $\sigma=1/3$, the values for E were determined as shown in Table 2. They are of the same order of magnitude as those obtained by uni-axial compression tests (2.5×10^8 and 2.8×10^8 N/m^2 (Takizawa, 1978)). The large value of L on Feb. 8th was probably caused by the hardening of ice due to the intense cold of 6-7 Feb. In fact, the ice thickness increased by 0.01 m (Table 2), and the ice temperatures on the 8th were lower than those on the 5th and 6th.

Table 2 Results of static loading tests

Date	h(m)	P(kg)	$\bar{\delta}$(mm)*	L(m)	$E(\times10^8$ N/m$^2)$	Remarks
Feb. 5	0.17	235	−5.4	2.3	6.1	Longi
6	0.17	235	−5.4	2.2	5.1	Longi
8	0.18	240	−3.5	2.7	9.8	Trans

* $\bar{\delta}$: Mean depression depth. Note that the deflection measurements were taken at a point 1 m from the center of the skidoo's trace. Longi : Longitudinal profile. Trans : Transversal profile.

III. 2 *Variation of deflection pattern with the load speed*

The records of typical runs are shown in Fig. 6 for various load speeds u. It was found that the deflection pattern, which changed with the speed, could be classified into the following five typical stages. It should be noted that the names of the five stages are tentative here ; they will be renamed in Section VII.

(1) Quasi-static stage ($0<u<3.5$ m/s). At low speeds, the deflection pattern was a dish-shaped depression surrounded by a slightly elevated rim. The overall pattern was similar to the static deflection profile shown in Fig. 5a. This fact suggests that the static profile is simply carried with the vehicle in this low speed range. It should be noted, however, that the center of the depression lagged behind the load.

(2) Early-transition stage ($3.5\leqq u<5.0$ m/s). As the speed was increased, the depression became deeper and narrower. The rim around the depression rose progressively, and a small trough began to form ahead of the forward rim.

(3) Late-transition stage ($5.0\leqq u<5.8$ m/s). With a further increase in speed, the depression continued to deepen and narrow, and a wave-like pattern began to form. The lag rapidly increased with the speed. These phenomena presaged a coming wave generation.

(4) Two-wave stage ($5.8\leqq u<8.0$ m/s). At speeds just above the critical speed u_c, two different waves were generated ; one with a shorter wavelength in front of the load (leading wave), and the other with a longer wavelength at the rear of it (trailing wave). Transforma-

tion of this time-deflection record into the spatial coordinates shows that a wave train extended for about 200 m. As described later in Section III.4, the critical speed was estimated to be 5.8 m/s. The depression was maximal in depth and minimal in width at u_c. With an increase in speed, the depression reversed its previous trend and became progres-

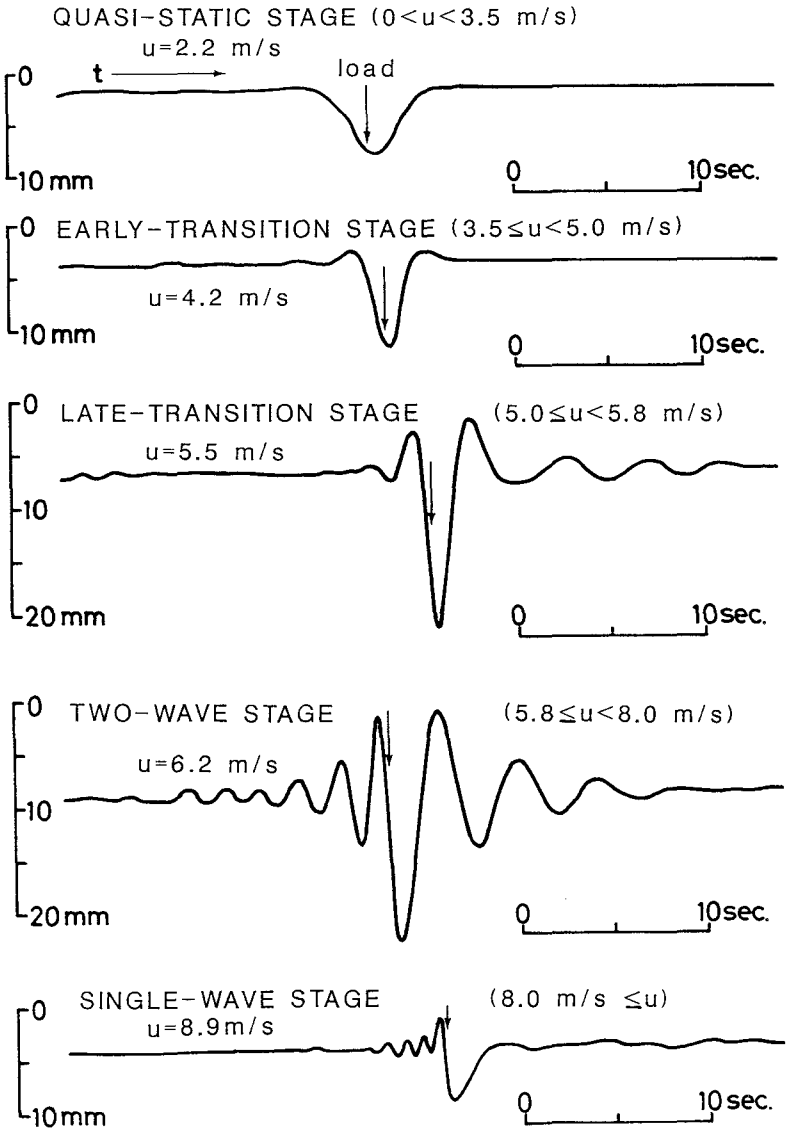

Fig. 6 Typical ice deflection records at various load speeds ; February 5, 1981.

sively shallower and wider. The wavelength of the leading wave was shortened and that of the trailing wave was elongated with an increase in speed. The number of wave crests (troughs) and the wave amplitude were reduced with increasing speed.

(5) Single-wave stage (8.0 m/s $\leqq u$). At a speed not much greater than u_c, the trailing wave disappeared and only the leading wave was observed. The depth of depression was smaller than those at $u=0$ m/s.

It should be emphasized that the two-wave stage existed ; in other words, the trailing wave was observed, though in a small region of speed. This wave was predicted by Wilson (1958) and later observed by Takizawa (1978), while it was not noticed in the other experiments conducted by Eyre and Hesterman (1976), Eyre (1977) and Beltaos (1979).

III. 3 *Propagation speed of deflection pattern*

Eyre (1977) mentioned that the speed of the generated ice wave was identical to the vehicle speed, because the vehicle maintained the same position relative to the ice deflection profile throughout each test run. In the present experiment, it was possible to evaluate the propagation speed of the generated depression and ice waves directly by making simultaneous recordings of the ice deflections at three locations along the track.

Figure 7 presents examples of the deflection records measured by the three deflectometers D_1-D_3 for three typical load speeds. The corresponding peaks, troughs and depression bottoms lie on one straight line, and the lines are parallel to each other. Hence this figure indicates that the steady-state was established, and the slope of the lines gives the propagation speed of the pattern. The relation obtained between the propagation speed and the load speed is shown in Fig. 8. Each value of the propagation speed was calculated by the average travelling time of distinct crests and the depression bottom of the pattern for a distance of 4 m between two deflectometers D_1 and D_3. The figure indicates that the deflection pattern was always propagated at the load speed at any stage, and accordingly, that when $u \geqq u_c$, the phase speed of the ice wave was identical with the load speed.

III. 4 *Depression depth*

The depression around the load did not lose its identity at all speeds, though its configuration changed with the speed, as shown in Fig. 6. At the bottom of the depression, the ice deflection was always maximal. The variation of the depression depth with the speed is shown in Fig. 9. The depth increased at first with the speed and reached its maximum, which demonstrated the existence of the critical speed u_c. At speeds above it, the depth decreased quickly with an increase in speed and then became comparable to the static values at $u \sim 1.5u_c$. With a further increase in speed, the depth continued to decrease gradually and its values were smaller than the static ones. The general trend of the variation is consistent with the previous experimental results (Wilson, 1958 ; Eyre, 1977 ; Takizawa, 1978 ; Beltaos, 1979 ; Squire *et al.*, 1985), and the theoretical prediction by Nevel (1970).

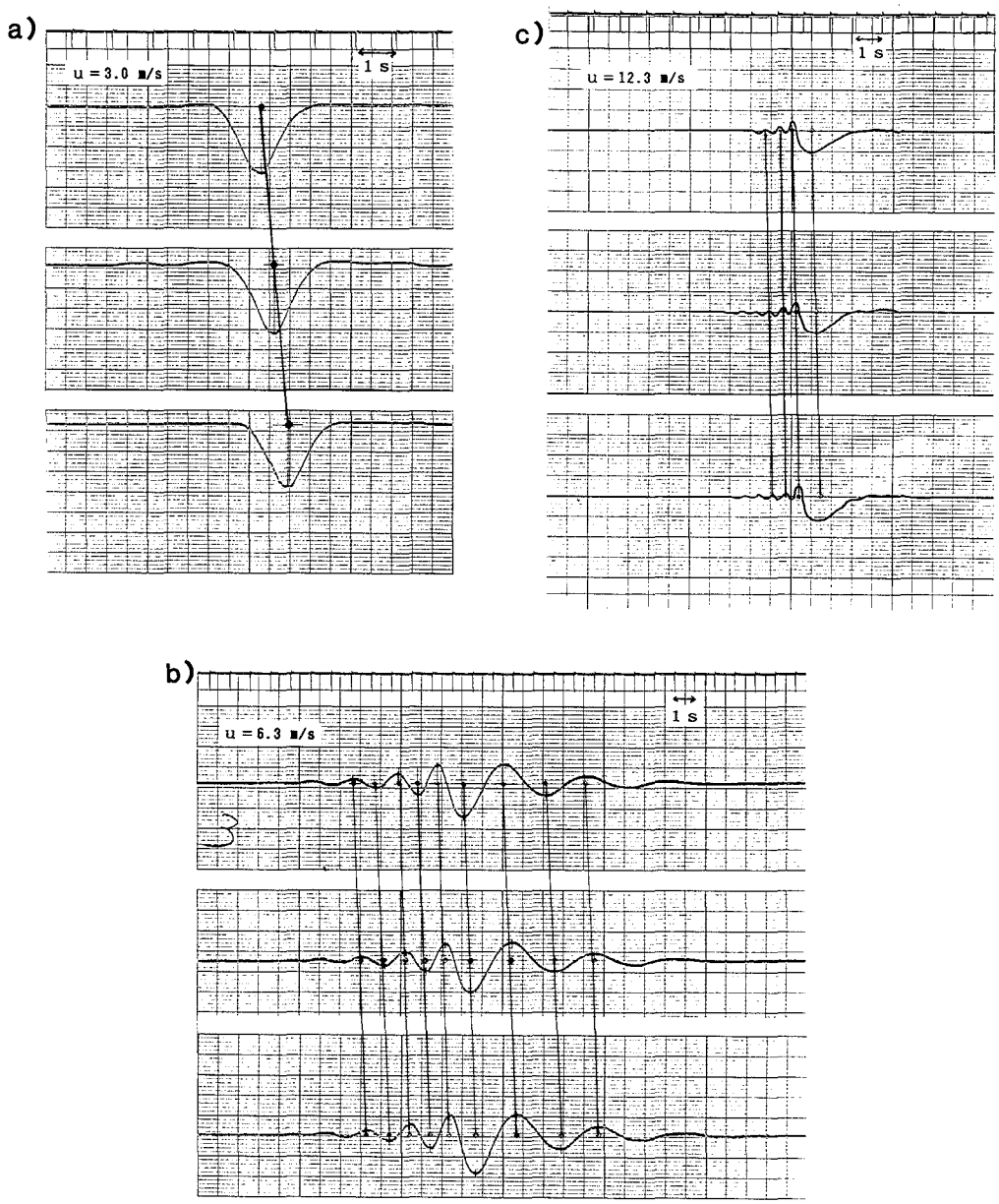

Fig. 7 Ice deflection records measured by three deflectometers, D_1-D_3, which were each installed at an interval of 2 m along the track (see Fig. 3). a) $u=3.0$ m/s, b) $u=6.3$ m/s, c) $u=12.3$ m/s.

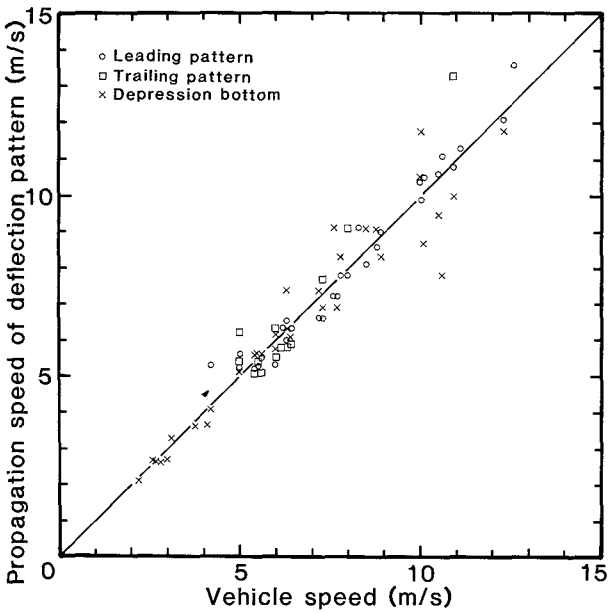

Fig. 8 Propagation speed of ice deflection pattern against the load speed. The distance between the deflectometer and the load's trace was 1 m.

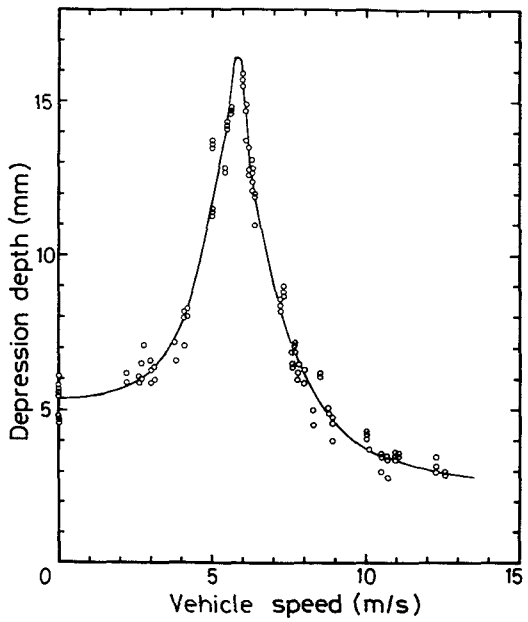

Fig. 9 Variation of depression depth, measured at a transversal distance of 1 m, with load speed.

As described above, the depression depth had a maximum, showing a prominent peak. This peak was used to determine the value for u_c. The data points and trend curve suggested that u_c was in the range of 5.6−6.0 m/s. Consequently, it was reasonable to take their mean, 5.8 m/s, as u_c.

The measured depth at u_c was about three times the depths under a static load, while according to the previous experiments, it was approximately two (Eyre, 1977 ; Beltaos, 1979) to four times (Takizawa, 1978).

III. 5 *Depression width*

The width of the depression curve was defined as the distance between the two points which intersected with the neutral line. The width also changed with the load speed, as shown in Fig. 10. It decreased at first with an increase in speed and reached its minimum at u_c ; above this value, the width increased rapidly and became greater than the width under a static load. The general trend is opposite to that of the depression depth shown in Fig. 9.

Equation (1) predicts a depression width of $7.8L$ when the load is at rest. For $L=2.2$ and 2.3 m (Table 2), the width was estimated to be 17.2 and 17.9 m, respectively. The width obtained from Fig.5a, however, is markedly smaller than the predicted values. As mentioned in the previous Section, the depth was almost the same at $u=0$ as at $u\sim1.5u_c$. If we assume that the width is also the same at $u=0$ as at $u\sim1.5u_c$, which is similar to the variation of the depth, the theoretical values seem to be reasonable. In addition, as will be shown in

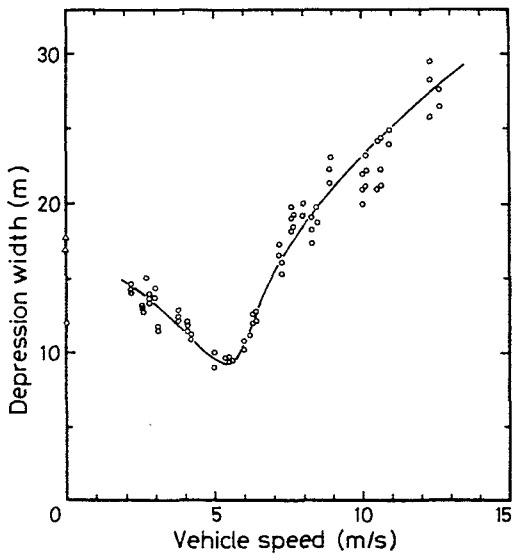

Fig. 10 Variation of depression width, measured at a transversal distance of 1 m, with load speed. △−theoretical values.

Section VI, an analytical solution for a moving load on an ice beam floating on water, including the effect of viscous damping, predicts that the width at $u=0$ is nearly equal to that at $u\sim1.5u_c$ for the case of small damping (see Fig. 28). Due to the lack of data points at low speeds, this large discrepancy cannot be explained.

III. 6 *Lag of the maximum deflection position behind the load*

As described earlier, the center of the depression lagged behind the load. The lag time t_l was transformed into the lag l by $l=ut_l$. The relationship between l, which was measured at a transversal distance of 1 m, and the load speed is presented in Fig. 11. The figure shows that l increased rapidly with u for $u>5$ m/s. This variation is identical to that found by Takizawa (1978). Meanwhile, at low speeds such as below 5 m/s, the lag was almost constant, about 1 m. This differs from the previous experimental results, which demonstrated that the lag arose at a speed slightly below u_c ; that is, at low speeds, the lag did not occur (Eyre, 1977 ; Takizawa, 1978). Furthermore, Beltaos' result (1979) indicated that the lag took place at $u>1.2u_c$. Two factors may cause a virtual lag : an experimental error and the effect of transversal distance. The experimental error, which was due to the delay in wire breaking of the skidoo detector, would make the lag decrease rather than increase. Thus it could not cause the virtual lag. Figure 12 shows a dependence of the lag on the transversal distance d between the deflectometer and the center of the skidoo's trace at various speeds. Seven speed groups were differentiated by different symbols. The results

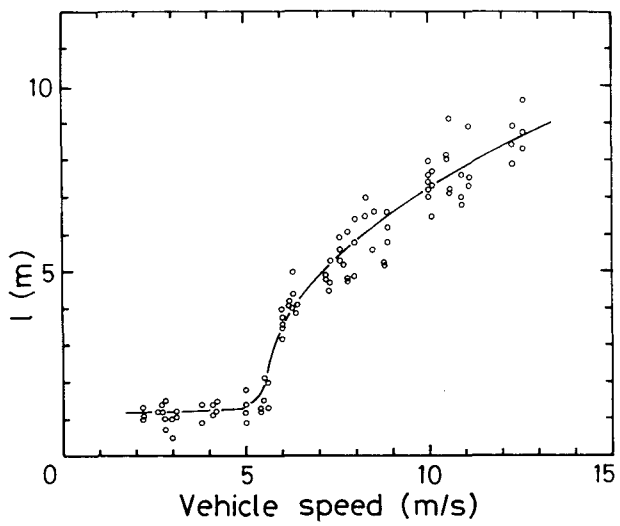

Fig. 11 Variation of the lag l, measured at a transversal distance of 1 m, with load speed.

showed that the lag decreased with decreasing d at every speed. Extrapolation of the data indicates that the lag is not zero at $d=0$ m, even for a speed of 2.9 m/s. Accordingly, we can conclude that the lag occurs at fairly low speeds. This conclusion is supported by the solution for a moving load on an ice beam, which will be presented in Section VI. As will be shown later in Fig.29, even at low speeds, the lag is not zero when the damping effect is taken into account. Moreover, the curve for the case of small damping is quite similar to the measured variation shown in Fig. 11. Thus it follows that the lag occurs for all speeds except 0 m/s, its magnitude is quite small for $u<u_c$, it increases markedly at a speed slightly below u_c and the variation can be explained in terms of small viscous damping. It should be noted that the lag is fairly small for $u<u_c$, which most likely explains why Eyre (1977), Takizawa (1978) and Beltaos (1979) did not notice it.

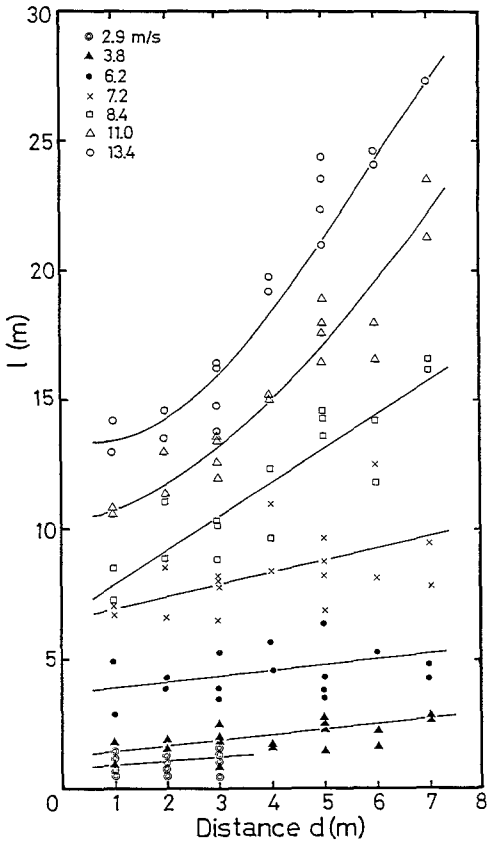

Fig. 12 Variation of the lag l with the transversal distance d for various speeds.

Figure 13 is a plot of the lag time t_l against u. The lag time decreased with increasing speed in the low speed range. The lag time increased abruptly at a speed slightly below u_c. At speeds above 6 m/s, it was almost constant and the mean lag time was 0.69 s. The lag time can be regarded as being related to the retardation time τ, which is one of the most important parameters in the viscoelastic theory. A drastic jump of t_l at a speed between 5−6 m/s would suggest that characteristic properties of the viscoelasticity of ice changed substantially at this speed range (at the late-transition stage).

Meanwhile, if we roughly assume that $\tau=t_l$, we can evaluate the viscosity coefficient for ice η, since τ is defined by $\tau=\eta/E$. The lag time is in the range of 0.2−0.8 s. Choosing $E_{\text{dynamic}}=3.5\times10^8$ N/m^2 for E (see Section IV.1), we have $\eta=7\times10^7-2.8\times10^8$ N·s/m^2. Taking the Maxwell unit as the viscoelastic model for sea ice, Tabata (1959) determined η by measuring the internal friction of rectangular ice bars. The values obtained were $3\times10^7-2\times10^8$ N·s/m^2 at ice temperatures around −3°C. The viscosity coefficients obtained in the present experiment, therefore, agree well with those by Tabata.

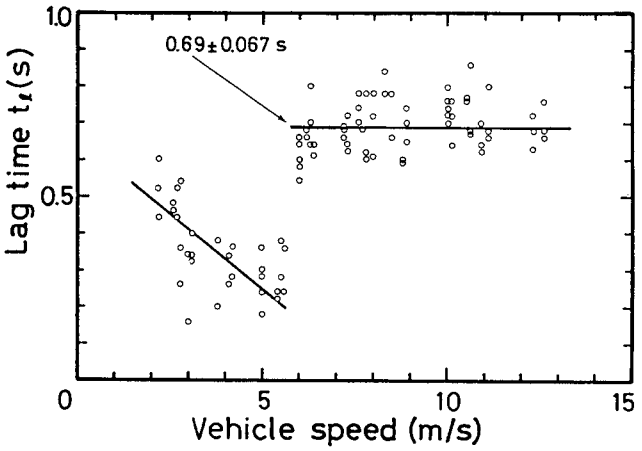

Fig. 13 Plot of the lag time t_L, measured at a distance of 1 m, against the load speed.

III. 7 *Wavelengths of ice waves*

The frequency of the ice wave f was determined directly from time-deflection records. The wave was found to be propagated with the load speed u ; hence, the wavelength λ was given by $\lambda = u/f$.

The variation of the wavelength with the speed is shown in Fig. 14. For the leading wave, λ decreased gradually with an increase in u. For the trailing wave, on the other hand, λ increased rapidly with u. The curve in the figure is a theoretical dispersion relation, which will be derived in the following Section.

IV. Ice wave characteristics and critical speed

IV. 1 *Dispersion relation of the ice wave due to a moving load*

Consider an infinite homogeneous and elastic ice sheet of thickness h and density ρ_i floating on water of density ρ_w. The upper undisturbed water surface is $z=0$ and the water bottom is $z=-H$. The differential equation describing the motion of the ice sheet is

$$D\nabla^4 w+\rho_i h\frac{\partial^2 w}{\partial t^2}-p=0, \tag{3}$$

where

$$\nabla^4=\frac{\partial^4}{\partial x^4}+2\frac{\partial^4}{\partial x^2\partial y^2}+\frac{\partial^4}{\partial y^4},$$

$$D=Eh^3/12(1-\sigma^2),$$

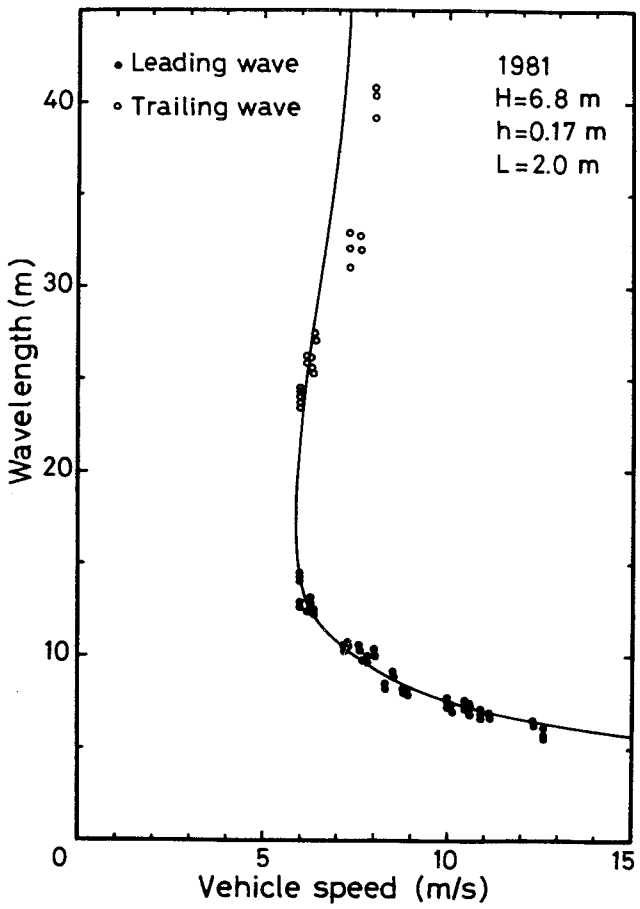

Fig. 14 Variation of wavelength with load speed. The distance between the deflectometer and the load's trace was 1 m.

w the vertical deflection of the ice, t the time, p the water pressure on the ice and x, y the horizontal axes.

Inviscid water is assumed and the water flow is taken to be irrotational with velocity potential ϕ.

$$\phi = A \cosh k(z+H) \cos k(x-ct), \tag{4}$$

where k is the wavenumber, c the phase speed.
This satisfies the equation of continuity in the water

$$\frac{\partial^2 \phi}{\partial x^2} + \frac{\partial^2 \phi}{\partial y^2} + \frac{\partial^2 \phi}{\partial z^2} = 0. \tag{5}$$

The boundary conditions are

$$\left.\frac{\partial\phi}{\partial z}\right|_{z=-H}=0, \tag{6}$$

$$\frac{\partial w}{\partial t}=\left.\frac{\partial\phi}{\partial z}\right|_{z=w}, \tag{7}$$

$$\left.\frac{\partial\phi}{\partial x}\right|_{x\to\pm\infty}=\left.\frac{\partial\phi}{\partial y}\right|_{y\to\pm\infty}=0, \tag{8}$$

$$\phi|_{x,y\to\pm\infty}=0. \tag{9}$$

Bernoulli's equation must be satisfied as a boundary condition at the ice-water interface. Linearized, Bernoulli's equation at $z=w$ is

$$p=-\rho_w g w-\rho_w\left.\frac{\partial\phi}{\partial t}\right|_{z=w}. \tag{10}$$

We consider uniform plane waves of the form

$$w=w_0\cos k(x-ct). \tag{11}$$

Noting that $|w|\ll H$, and combining eqs. (4), (7) and (11), we obtain

$$A=w_0 c/\sinh kH. \tag{12}$$

Substitution of eqs. (4) and (10)–(12) into eq. (3) yields

$$c^2=\frac{Dk^3/\rho_w+g/k}{\rho_i h\,k/\rho_w+\coth kH}. \tag{13}$$

This is the dispersion relation for free waves in the floating ice sheet. The very short waves are out of the scope of the present paper. Thus, noting that $\rho_i hk/\rho_w\ll 1$ $(\lambda>h)$ and $\coth kH\geqq 1$, we have the dispersion relation for all waves except very short ones.

$$c^2=\frac{g}{k}(1+L^4k^4)\tanh kH, \tag{14}$$

$$L=\left[\frac{D}{\rho_w g}\right]^{1/4}=\left[\frac{Eh^3}{12\rho_w g(1-\sigma^2)}\right]^{1/4}. \tag{15}$$

As described in Section III.3, the phase speed of ice waves is equal to the load speed. Furthermore, Kerr (1983) showed theoretically that $c=u$ and the minimum phase speed c_{min} is the same as the critical speed u_c. A physical interpretation of $c_{min}=u_c$ will be given later. Hence c in eq. (14) can be replaced by u. Noting that $k=2\pi/\lambda$, we obtain the dispersion relation between the wavelength λ and the load speed u for the waves induced by a moving load.

$$u^2=\frac{g\lambda}{2\pi}\left[1+L^4\left(\frac{2\pi}{\lambda}\right)^4\right]\tanh\left(\frac{2\pi}{\lambda}H\right). \tag{16}$$

The curve in Fig. 14 represents eq. (16) for the best-fit $L=2$ m in the least squares sense. It describes the measured variation of λ with u very well. It is noted that the value of L is slightly smaller than those obtained by the static loading tests (see Table 2). Consequently, the corresponding value for the elastic modulus E_{dynamic} calculated through eq. (15) for $h=$ 0.17 m is 3.5×10^8 N/m^2 and is smaller than E_{static}. It is known that the E values determined by dynamic methods are generally larger than those by static ones. However, since the E values are strongly affected by the test conditions and scatter considerably (Weeks and Assur, 1967), this opposite result is attributable to the scattering and probably has no significant meaning.

Equation (16) indicates that the dispersion curve also depends on the water depth H. Figure 15 is a non-dimensional plot of the experimental results of Takizawa (1978), and it gives two theoretical curves for $H=6.2$ and 12 m. The non-dimensional speed U and

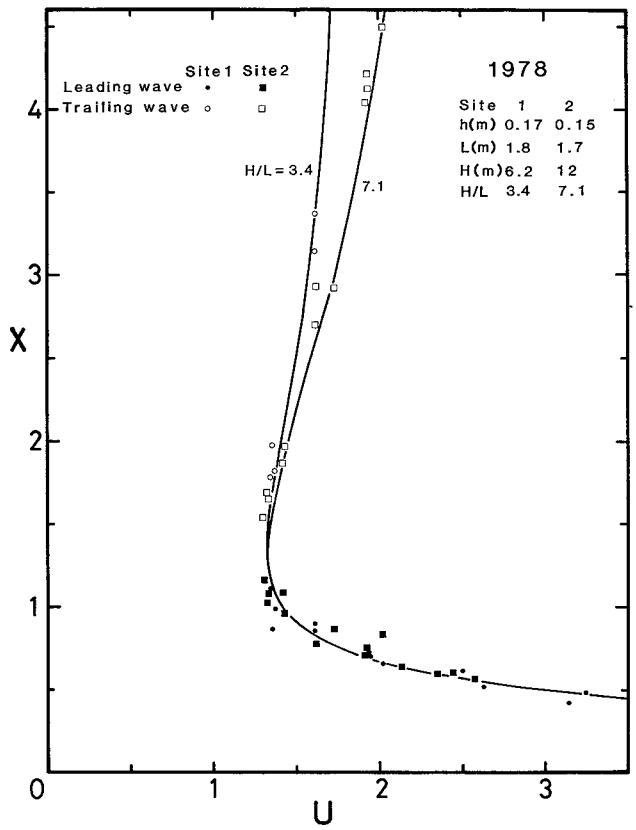

Fig. 15 Non-dimensional plot of dispersion relation obtained by a field experiment in 1978 carried out at two sites with different water depths.

wavelength X will be defined in the following Section. The two curves for $H/L=3.4$ ($H=$ 6.2 m) and 7.1 ($H=12$ m) agree fully with the data points at two experimental sites with different water depths, respectively. It is verified that, therefore, the theoretical relation of eq. (16) can represent satisfactorily the experimental results. Thereupon, from eq. (16) we can evaluate the critical speed, which will be described in next.

IV. 2 *Evaluation of the critical speed*

To simplify the mathematics, the non-dimensional load speed U and wavelength X are defined as follows :

$$U=u/\sqrt{gL},\ X=\lambda/2\pi L. \tag{17}$$

Substitution of eq. (17) into eq. (16) yields the non-dimensional dispersion relation

$$U^2=(X+1/X^3)\tanh\left(\frac{H}{L}\frac{1}{X}\right). \tag{18}$$

Since $c_{\min}=u_c$, a necessary condition for locating the non-dimensional critical speed U_c is $dU/dX=0$. It gives the expression

$$X_c=\left[\frac{3+(2\frac{H}{L}\frac{1}{X_c})/\sinh(2\frac{H}{L}\frac{1}{X_c})}{1-(2\frac{H}{L}\frac{1}{X_c})/\sinh(2\frac{H}{L}\frac{1}{X_c})}\right]^{1/4}, \tag{19}$$

where X_c is X for U_c.

Solving eq. (19) numerically, U_c and X_c are expressed as a function of H/L (Fig. 16). The theoretical curve for U_c shows close agreement with the experimental results. When H and L are known, therefore, this diagram predicts U_c. It may be seen from the figure that U_c is practically constant for $H/L>3$. Since large H/L is equivalent to "deep water", which means that the water is deep in comparison with L or ice thickness h, we can put $U_c=$ 1.32 with enough accuracy for deep water. From eq. (17), accordingly, the critical speed u_c for deep water is

$$u_c=1.32\sqrt{gL}. \tag{20}$$

Thus, given h and E, we can evaluate u_c from eq. (20).

When this evaluation of u_c is used in practice, H is known in most cases, which leaves h and E to be estimated. Fairly correct values of h can be obtained by making direct measurements ; which is undoubtedly the best method. However, if this is difficult, an indirect approach is available ; that is, a prediction of h by an empirical formula that expresses a relationship between ice thickness and cumulative degree-days below freezing. Given the air temperatures, the previously established formula provides fairly accurate values of ice thickness. On the other hand, measurements of the elastic modulus are not easy, and moreover, its values show a marked scattering (Weeks and Assur, 1967). Figure

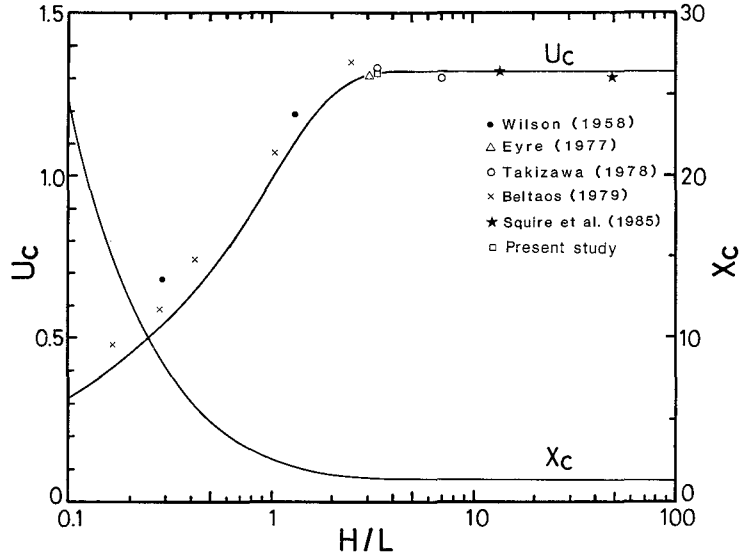

Fig. 16 Non-dimensional critical speed U_c and non-dimensional wavelength X_c, X for U_c, as a function of H/L. Experimental results for U_c from various sources are also plotted.

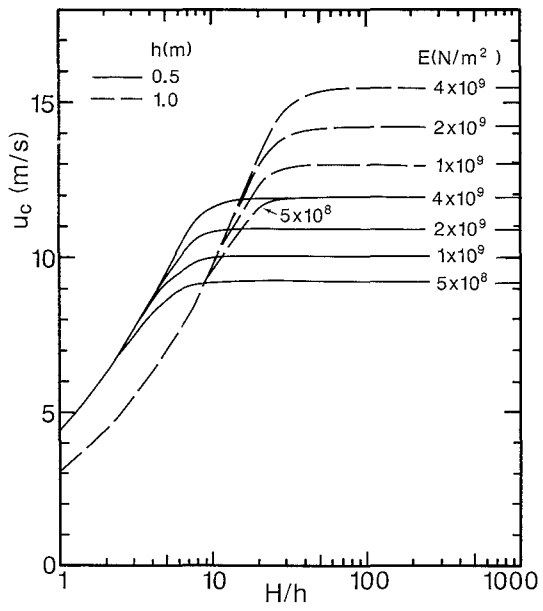

Fig. 17 Dependency of the critical speed u_c on the elastic modulus E for the ice thickness $h=0.5$ m and 1.0 m.

17 demonstrates a dependency of u_c on E for $h=0.5$ and 1.0 m. If E is doubled for a fixed h, the critical speed is increased by about 10 % at most. Meanwhile, if h is doubled for a fixed E, it is increased by as much as 30−40 %. Hence a change of E produces a much smaller effect on u_c than that of h. It follows from this that accurate predictions of h are invaluable ; in other words, a rough estimation of E may be pertinent to this problem. Particularly, when H/h is small, which denotes shallow water, the curves for various E are superimposed. Accordingly, we have here a very convenient result that any value of E is adequate to predict u_c for shallow water.

IV. 3 *What assigns the positions of ice waves ?*

Figure 14 indicates that two waves with different wavelengths may be propagated at the same speed and that a shorter wave appears in front of the load and a longer one at the rear. It should be noted that eqs. (16) or (18) do not specify the positions of the two waves. Then, what assigns their positions ? A solution can be given by the group velocity and the existence of minimum phase speed. It also offers a physical explanation for $c_{\min}=u_c$. The property of dispersive waves is that the group velocity with which energy is propagated is different from the phase speed. Equation (18) may be differentiated to obtain the non-dimensional group velocity C through the relation

$$C=U-X(\mathrm{d}U/\mathrm{d}X), \tag{21}$$

and we have

$$C=U\left[1+\frac{3/X^4-1}{2(1+1/X^4)}+\frac{H/LX}{\sinh\left(\frac{H}{L}\frac{1}{X}\right)}\right]. \tag{22}$$

Figure 18 is a schematic plot of U and C. As the load moves across the ice sheet, ice waves are generated with wavelengths (X_1 and X_2) appropriate to the speed U, which is equivalent to the wave speed. A longer wave with X_2 has $C_2<U$, so that the energy travels at a speed C_2 less than U. The energy in this wave, therefore, always lags behind the load. Accordingly, the longer wave is found behind the load. By contrast, a shorter wave with X_1 has $C_1>U$, so that its energy travels in front of the load. The shorter and the longer wave, therefore, are found in different positions : ahead of and behind the load, respectively.

Remembering that a necessary condition for locating U_c is $\mathrm{d}U/\mathrm{d}X=0$, we find from eq. (21)

$$C|_{X=X_c}=U_c, \tag{23}$$

namely, the group velocity is equal to the critical speed U_c (= minimum phase speed) at $X=X_c$. Thus, it follows that energy due to a load moving at U_c travels at the same speed as U_c, so that it cannot escape from the load. Accordingly, energy will accumulate continuously

underneath the load, and this accumulation causes the marked amplification of ice deflection at U_c. Therefore, the critical speed necessarily coincides with the minimum phase speed. This is a simple explanation for the existence of the critical speed.

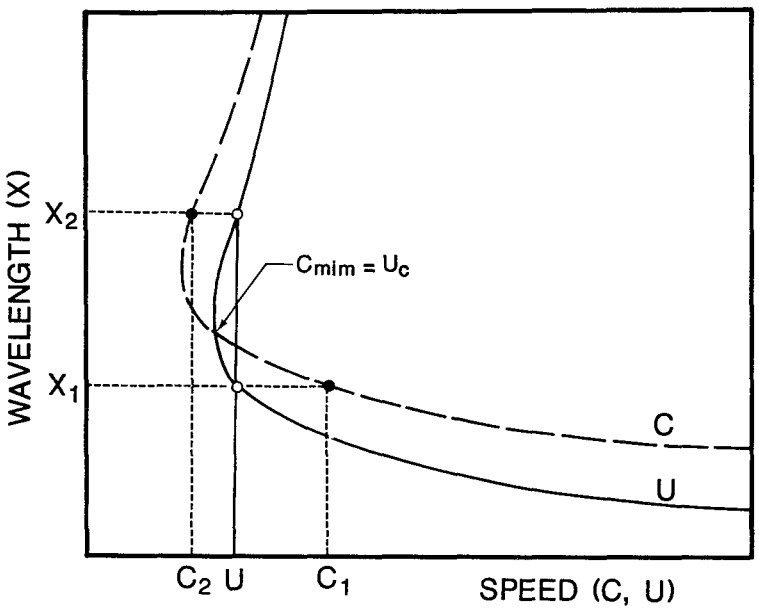

Fig. 18 Schematic plot of non-dimensional group velocity C and load speed U as a function of wavelength.

V. Spatial characteristics of ice deflection pattern

V.1 *Three-dimensional images of ice deflection*

Three graphic displays of the three-dimensional images of ice deflection are presented in Fig.19. Each display was synthesized from three records with different transversal distances between the deflectometers and the skidoo's trace. At a low speed (Fig. 19a), the depression becomes shallower with the transversal distance. At a speed just above the critical speed (Fig. 19b), there is a well-defined wave train. Wave crests appear to become higher with the transversal distance. At a high speed (Fig. 19c), it is clear that the height of a wave crest increases with the distance, while the depth of the depression decreases. It can be seen that the depression line is not perpendicular to the direction of motion. This feature has already been illustrated in Fig. 12. The solid lines in the figure can be considered to

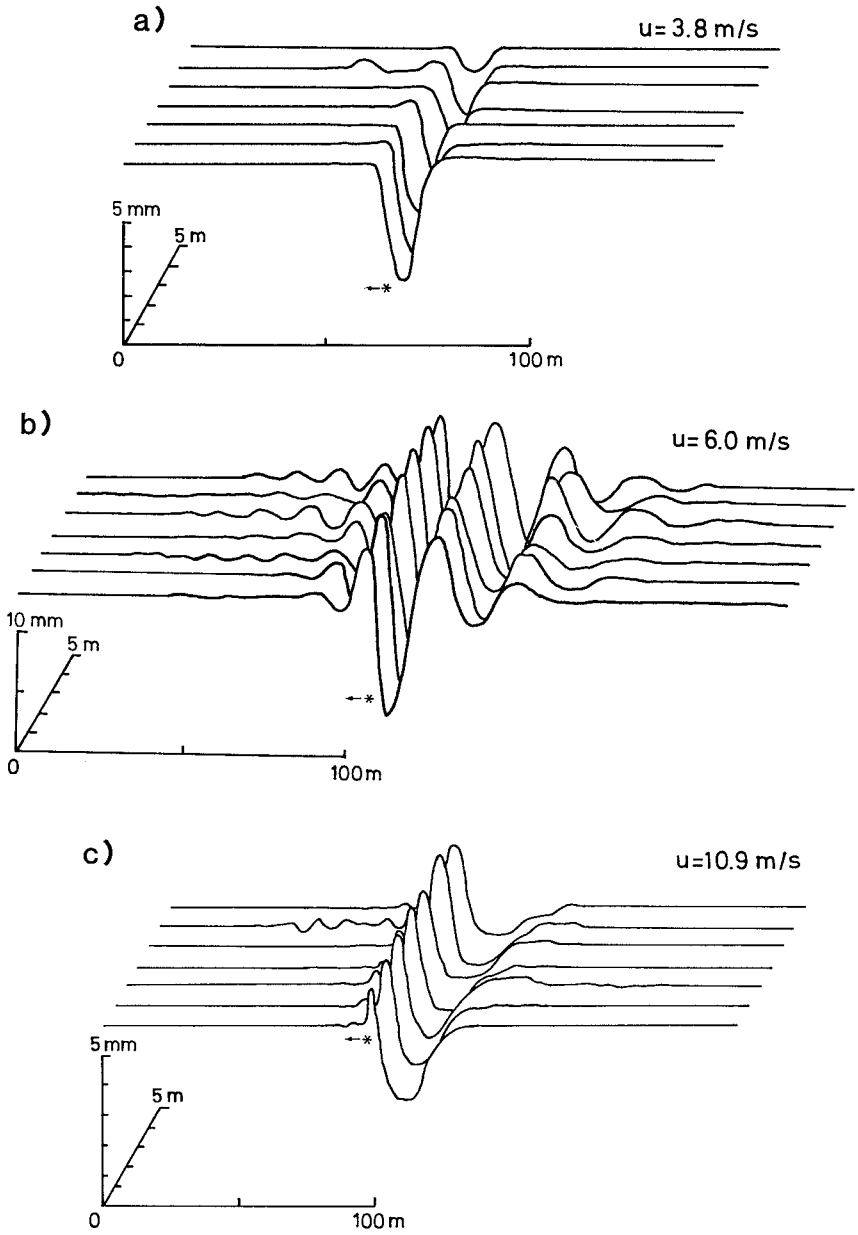

Fig. 19 Three-dimensional images of ice deflection. Each display was synthesized from three test runs with different transversal distances.

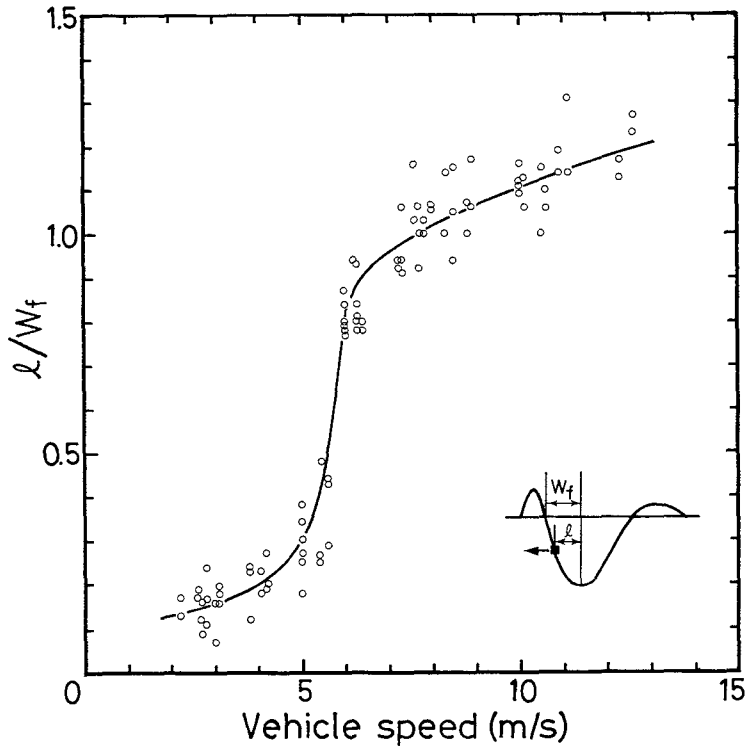

Fig. 20 Ratio of the lag l to the forward half of the depression width W_f against load speed. The distance between the deflectometer and the load's trace was 1 m.

show a plan view of the depression lines at the time when the load moving along the ordinate downward reached the origin. It is obvious that the depression lines are oblique to the direction of motion even at fairly low speeds, and that the angle between them becomes sharp with increasing speed. In addition, Davys *et al.* (1985) predicted that wave crests are convex to the direction of a vehicle's motion (see Fig.23).

V. 2 *Load's position with respect to the depression profile*

The ratio of l to the forward half of the width W_f is shown in Fig. 20. The ratio indicates the relative position of the load with respect to the depression curve. That the ratio is zero means that the load is situated in the center of the depression, and when the ratio is 1.0, it is just in the position of the neutral line.

The load remained slightly ahead of the depression bottom when its speed was below the critical speed. At speeds near the critical speed, it shifted forward along the depression slope. For speeds more than 8 m/s, the ratio was larger than 1.0. This indicates that at

high speeds, the ice beneath the load was not depressed but was somewhat elevated.

V. 3 *Spatial nature of wave amplitude*

Figure 21 shows variations of the height of the forward rim of the depression and the depression depth with the transversal distance from the load. As mentioned before, the height increased with the distance at all speeds but the low speed $u=3.8$ m/s. The depth, on the other hand, decreased with an increase in distance at all speeds. Figure 22 demonstrates the height of the first peak (height of backward rim) and the depth of the first trough of the trailing wave against the transversal distance. Both the height and the depth increased with

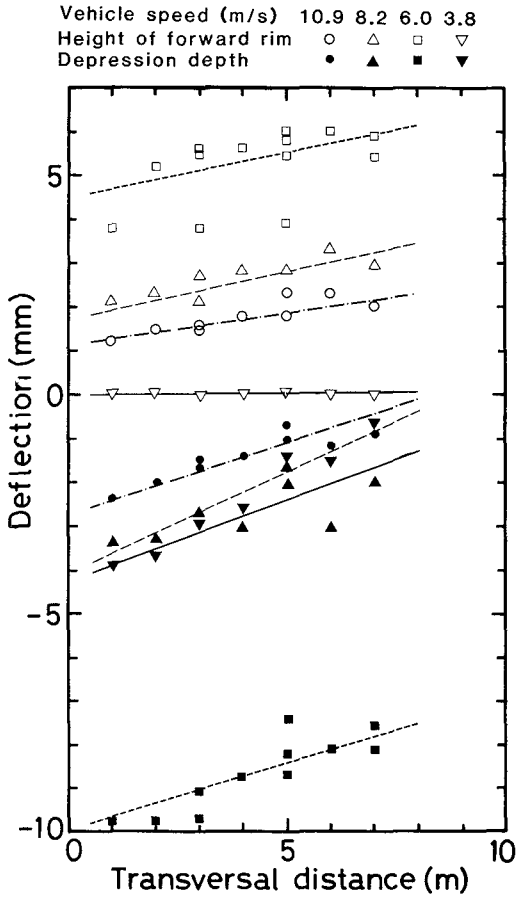

Fig. 21 Variation of height of the forward rim of the depression and the depression depth with the transversal distance from the load.

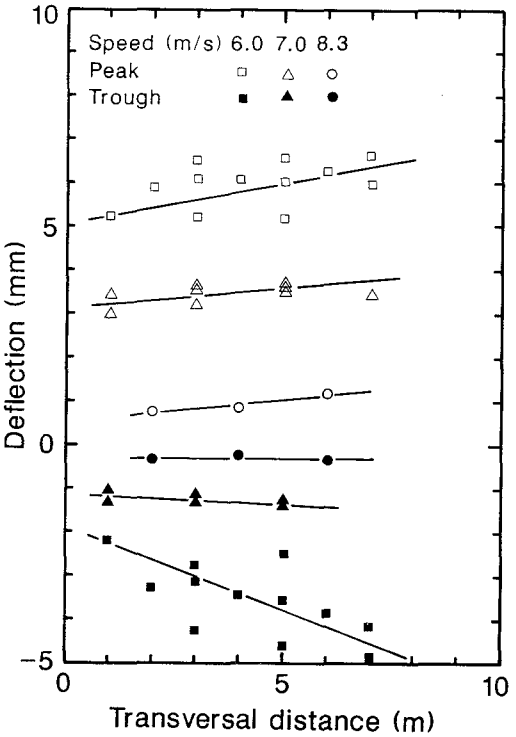

Fig. 22 Variation of height of the first peak and depth of the first trough of the trailing wave with the transversal distance.

the distance, except for the depth at $u=8.3$ m/s. The peak-to-trough height increased with the distance at all speeds ; that is, the wave amplitude became larger with the distance. This would appear to be an unlikely occurrence. Davys *et al.* (1985) presented some graphs of wave amplitude at a constant radial distance against θ, the angle from the direction of the motion of load. As θ changed from 0° to 180°, the amplitude increased gradually and showed a prominent peak at around 160°, and above it the amplitude decreased rapidly. In other words, the amplitudes at the rear left and right of the load were larger than that just behind it (see Fig. 10 in Davys *et al.* (1985)). The present experimental results shown in Fig. 22, therefore, support their theoretical prediction. As for the variation of the forward rim in Fig. 21, it should be interpreted as further evidence for the above. The depression depth, on the other hand, displayed the opposite tendency. This would suggest that the depression is a singular zone in the two-dimensional wave field.

V.4 *Why the single-wave stage appears ?*

Let us now consider why the single-wave stage appeared, though eq. (16) predicts the existence of two waves at all speeds for $u \geqq u_c$. The two-dimensional wave patterns given by Davys *et al.* (1985) most likely answer this question. They showed that at speeds $u \geqq V_c$, a shadow zone appears behind the load (Fig. 23). The speed V_c is the phase speed of a shallow water wave and is equal to $\sqrt{gH}$. The ice deflection measurements in the present experiment were made in the neighborhood of the center line of the load's trace. Hence the obtained records shown in Fig. 6 correspond to deflection patterns in the narrow strip along the x-axis (hatched area) in Fig. 23. No wave, therefore, was observed behind the load at

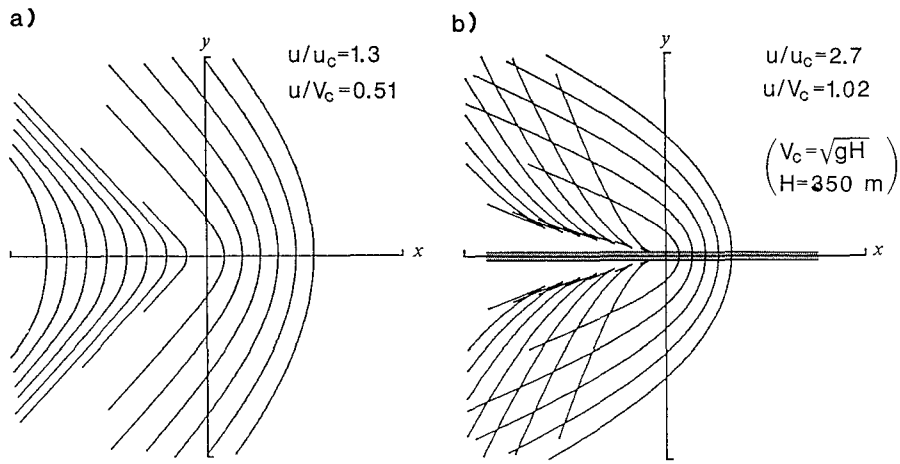

Fig. 23 Wavecrest pattern for a) $u=30$ m/s ($u/u_c=1.3$, $u/V_c=0.51$) ; b) $u=60$ m/s ($u/u_c=2.7$, $u/V_c=1.02$). Ice thickness is 2.5 m and water depth is 350 m. (from Davys *et al.*, 1985).

speeds $u \geqq V_c$. Presumably this is the reason why the trailing wave disappeared at high speeds. This explanation is supported by the fact that the characteristic speed V_c in the present experiment is 8.2 m/s, and this speed is nearly equal to the boundary speed of 8.0 m/s between the two-wave stage and the single-wave stage. Thus, it follows that two ice waves are inherent in the response of floating ice sheets to moving loads ; but because of the existence of the shadow zone behind the load at $u \geqq V_c$, an observer close to the load's trace will seemingly find out a single-wave stage.

The other possible cause that veiled the trailing wave is a turbulent wake in the water. It is reasonably expected that a high-speed moving load created intensive hydrodynamic pressure disturbances in its wake, so that the miss-matching occurred between ice-motion and water-motion. As a result, the primary ice motion (the trailing wave) would be canceled out and no waves other than random or irregular deflection patterns would be observed behind the load.

Both causes probably contributed to the appearance of the single-wave stage. The question whether or not the above mentioned explanations are pertinent or whether another one is required should be addressed in a future field experiment.

V.5 *Two-dimensional wavenumber space and wave pattern*

The detailed theoretical work of Davys *et al.* (1985) presented two-dimensional wavenumber curves which give the wave patterns. They were derived through a rigid and rather complex mathematical treatment. If we are concerned with only the wavenumber curves, a simple and direct alternative way is available. Denote the two-dimensional wavenumber vector $\boldsymbol{k}$ by

$$\boldsymbol{k}=(k_x, k_y),\ k=(k_x^2+k_y^2)^{1/2}. \tag{24}$$

From eq. (14), the general expression of the dispersion relation for the two-dimensional free waves may be written in terms of the angular frequency ω

$$\omega^2=g\sqrt{k_x^2+k_y^2}[1+L^4(k_x^2+k_y^2)^2]\tanh\sqrt{k_x^2+k_y^2}H, \tag{25}$$

where $\omega=ck=c(k_x^2+k_y^2)^{1/2}$.

It should be noted that in Section IV, we discussed implicitly the case where $k_y=0$; namely, $k=k_x$. In the strict sense, therefore, the dispersion relation eq. (16) was for waves induced by a moving *line* load.

The angular frequency ω of waves generated by sources traveling with constant speed u along x-axis in the positive direction and oscillating at fixed angular frequency ω_0 is expressed by

$$\omega=\omega_0+k_x u, \tag{26}$$

(Lighthill (1978), ch. 4). Ship waves are given as a principal example of waves of this kind.

We here consider the case $\omega_0=0$. Substitution of eq. (26) into eq. (25) yields

$$k_x^2u^2=g\sqrt{k_x^2+k_y^2}[1+L^4(k_x^2+k_y^2)^2]\tanh\sqrt{k_x^2+k_y^2}H. \tag{27}$$

Defining $K_x=k_xL$, $K_y=k_yL$, $U=u/\sqrt{gL}$, the non-dimensional equation becomes

$$U^2K_x^2-\sqrt{K_x^2+K_y^2}[1+(K_x^2+K_y^2)^2]\tanh\frac{H}{L}\sqrt{K_x^2+K_y^2}=0. \tag{28}$$

This equation gives wavenumber curves, describing ice waves induced by a moving *concentrated* load with constant speed, for various values of U and H/L. Figure 24 is an example of wavenumber curves applied to the present work. Only waves with wavenumbers lying on the curve will appear in the steady pattern. The wave crest at P is normal to wavenumber vector $\boldsymbol{k}$ and the group velocity is normal to the curve. Angle β is the angle between $\boldsymbol{k}$ and the direction of the moving load, and Q on the curve is the point such that OQ is a tangent. A segment at the left of Q represents the trailing waves and that at the right of Q the leading waves. Thus, we can obtain the wave patterns in all cases through eq. (28). Figure 24 gives the same wave patterns as those from Davys *et al.* (1985) shown in Fig. 23, which agreed well with the experimental results. For a detailed interpretation of the wavenumber curve, the reader is referred to Lighthill (1978, ch.4).

Figure 24 indicates that as a load is passing by, an observer at some distance from the

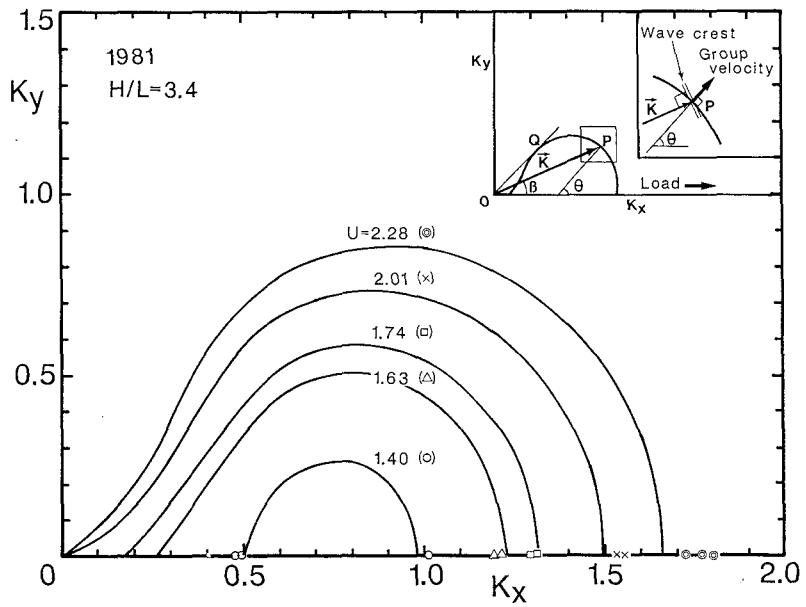

Fig. 24 Non-dimensional wavenumber curves for various speeds U, when $H/L=3.4$.

test track will notice a change in the wavenumber of generated waves ; namely, the wavenumber shifts with the direction of observation point from the moving load, θ, varying approximately from 0° to 180°. In cases where the observation point is located beside the track (the present experiment is a typical one), θ is close to 0° or 180°, except for a few seconds when the load just passes by the observation point. Consider the obtained record at $u=6.2$ m/s, shown in Fig. 6, as an actual example. The distance between the center line of the load's trace and the deflectometer (observation point) was 1 m (Fig. 25). The points where θ was 10° (170°) and 5° (175°) were only 5.7 m and 11.4 m away from the deflectometer along the track. These distances corresponded to 0.9 s and 1.8 s, respectively, for $u=6.2$ m/s. Accordingly, the segment of ice deflection record such that $5°<\theta<175°$ was a period of 3.6 s occurring between the points 1.8 s before and after the instance the load passed the deflectometer. It is clear from Fig. 6 that this segment is very short and that substantial parts of the waves are outside of it. The segment such that $10°<\theta<170°$ is much shorter. Therefore, it follows that θ for the leading wave and the trailing wave can be approximated to 0° and 180°, respectively. This fact certifies that the one-dimensional model was appropriate to discuss the generated wave characteristics. When $\theta=0°$ and 180°, equation (25) is the same as eq. (14), since $k_y=0$. Hence the observed wavenumbers plotted in Fig. 24 as examples show a good agreement with the curves. Note that when an observation point is far away from the track, the dependency of the wavenumber on θ will become noticeable.

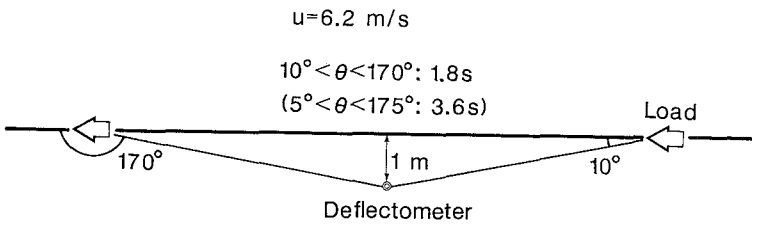

Fig. 25 Influence of change of the direction of observation point from the moving load on the wavenumber shift.

VI. Effect of viscous damping

As ice is a typical viscoelastic substance, in a strict sense, viscoelasticity must be included in the equation of motion. The four-parameter model (Maxwell unit and Voigt unit in series) is generally taken as the viscoelastic model for ice (e.g., Squire and Allan, 1980 ; Bates and Shapiro, 1981). This model, however, yields a very complex differential equation that is difficult to solve. The most common and simple approach is to assume that the damping force is proportional to the vertical velocity (viscous damping).

We now discuss the effects of viscoelasticity on ice deflection using this simple model. Consider an infinite ice beam floating on water. The equation of motion of the beam is

$$EI\frac{\partial^4 w}{\partial x^4}+\rho_i h\frac{\partial^2 w}{\partial t^2}+b\frac{\partial w}{\partial t}-p=P\delta(x-ut), \tag{29}$$

where I is the inertia moment of the beam, x the distance along the beam, b the coefficient of viscous damping, P the concentrated load that moves at a constant speed u along the x-axis, δ the delta function. Neglecting the $\rho_w\frac{\partial\phi}{\partial t}$ term in the linearized Bernoulli's equation of (10), we have

$$p=-\rho_w g w. \tag{30}$$

Before discussing the solution of eq. (29), we derive first the dispersion relation for free waves of the form

$$w(x, t)=w_0\cos k(x-ct). \tag{31}$$

Substituting eq. (31) into eq. (29) with $b=0$ and $P=0$, and using eq. (30), we have

$$c^2=\frac{g'}{k^2}(1+N^4k^4), \tag{32}$$

where $g'=\rho_w g/\rho_i h$ and $N^4=EI/\rho_w g$.
The minimum phase speed c_{min} and the wavenumber for c_{min}, k_c are

$$c_{min}=\sqrt{2g'}N, \tag{33}$$

$$k_c=1/N. \tag{34}$$

Remembering that $u=c$ and $u_c=c_{min}$, and denoting $M=u/u_c$ and $K=k/k_c$, we have the non-dimensional dispersion relation

$$M^2=(K^2+1/K^2)/2. \tag{35}$$

Returning now to the consideration of a damped ice beam subjected to a moving load, we introduce here a new coordinate system (x', z', t') that moves with the load. We further assume that the load has moved at a constant speed for a sufficient length of time, that transient motions of the ice-water system have disappeared, and, accordingly, that only the steady state motion remains. Upon defining the new system as

$$x'=x-ut,\ z'=z,\ t'=t, \tag{36}$$

and then dropping the primes, equation (29) becomes

$$N^4\frac{\mathrm{d}^4 w}{\mathrm{d}x^4}+\frac{u^2}{g'}\frac{\mathrm{d}^2 w}{\mathrm{d}x^2}-\left(\frac{b\ u}{\rho_w\ g}\right)\frac{\mathrm{d}w}{\mathrm{d}x}+w=\frac{P}{\rho_w g}\delta(x). \tag{37}$$

From the analogy of the simple spring mass system, critical damping b_c may be defined by

$$b_c=2(\rho_w g\rho_i h)^{1/2}. \tag{38}$$

Setting $B=b/b_c$ and noting eq. (33), equation (37) can be rewritten

$$\frac{d^4w}{dx^4}+2\frac{M^2}{N^2}\frac{d^2w}{dx^2}-2\sqrt{2}\frac{BM}{N^3}\frac{dw}{dx}+\frac{w}{N^4}=\frac{P}{EI}\delta(x). \tag{39}$$

The simplest method of solving eq. (39) is to set the right-hand side equal to zero and to incorporate the concentrated load P through the matching conditions at $x=0$. Thus the differential equation that should be solved is

$$\frac{d^4w}{dx^4}+2\frac{M^2}{N^2}\frac{d^2w}{dx^2}-2\sqrt{2}\frac{BM}{N^3}\frac{dw}{dx}+\frac{w}{N^4}=0. \tag{40}$$

Assuming $w=Ce^{mx}$, and substituting it into eq. (40), we obtain

$$m^4+\frac{2M^2}{N^2}m^2-\frac{2\sqrt{2}BM}{N^3}m+\frac{1}{N^4}=0. \tag{41}$$

Descartes' rule of signs provides that eq. (41) cannot have more than one pair of real roots. Thereupon let us assume the following four complex roots,

$$\left.\begin{aligned} m_1&=a+ib_1,\\ m_2&=a-ib_1,\\ m_3&=-a+ib_2,\\ m_4&=-a-ib_2. \end{aligned}\right\} \tag{42}$$

They must satisfy eq. (43)

$$(m-m_1)(m-m_2)(m-m_3)(m-m_4)=0. \tag{43}$$

Substitution of eq. (42) into eq. (43) yields

$$m^4+(-2a^2+b_1^2+b_2^2)m^2-2a(b_2^2-b_1^2)m+(a^2+b_1^2)(a^2+b_2^2)=0. \tag{44}$$

Comparing the coefficients of eqs. (41) and (44), it follows that

$$-2a^2+b_1^2+b_2^2=2M^2/N^2, \tag{45}$$

$$-2a(b_2^2-b_1^2)=-2\sqrt{2}BM/N^3, \tag{46}$$

$$(a^2+b_1^2)(a^2+b_2^2)=1/N^4. \tag{47}$$

From eqs. (45) and (46)

$$b_1^2=\frac{M^2}{N^2}+a^2-\frac{BM}{\sqrt{2}aN^3}, \tag{48}$$

$$b_2^2=\frac{M^2}{N^2}+a^2+\frac{BM}{\sqrt{2}aN^3}. \tag{49}$$

Substituting eqs. (48) and (49) into eq. (47), we have

$$a^6+\frac{M^2}{N^2}a^4+\frac{M^4-1}{4N^4}a^2-\frac{B^2M^2}{8N^6}=0. \tag{50}$$

Hence the positive real root of eq. (50) for a and eqs. (48) and (49) give a solution for eq. (40) in the form of eq.(42). Rewritten in the real form, the solution becomes

$$w=e^{-ax}(C_1 \sin b_2x+C_2 \cos b_2x)+e^{ax}(C_3 \sin b_1x+C_4 \cos b_1x). \tag{51}$$

The boundary conditions are

$$w|_{x\to\pm\infty}=\frac{dw}{dx}\Big|_{x\to\pm\infty}=0. \tag{52}$$

Thus, from eq. (52)

$$w_+=e^{-ax}(C_1 \sin b_2x+C_2 \cos b_2x),\ x>0 \tag{53a}$$
$$w_-=e^{ax}(C_3 \sin b_1x+C_4 \cos b_1x),\ x<0 \tag{53b}$$

The remaining four constants C_1-C_4 can be determined from the matching conditions at $x=0$.

$$w_+(0)=w_-(0), \tag{54a}$$

$$\frac{dw_+}{dx}\Big|_{x=0}=\frac{dw_-}{dx}\Big|_{x=0}, \tag{54b}$$

$$\frac{d^2w_+}{dx^2}\Big|_{x=0}=\frac{d^2w_-}{dx^2}\Big|_{x=0}, \tag{54c}$$

$$\left(\frac{d^3w_+}{dx^3}-\frac{d^3w_-}{dx^3}\right)\Big|_{x=0}=\frac{P}{EI}. \tag{54d}$$

The determined constants are

$$\left.\begin{aligned} &C=C_2=C_4=-\frac{4aP}{EI[8a^2(2a^2+b_1^2+b_2^2)+(b_1^2-b_2^2)^2]},\\ &C_1=\frac{(b_1^2-b_2^2+4a^2)}{4ab_2}C,\ C_3=\frac{(b_1^2-b_2^2-4a^2)}{4ab_1}C. \end{aligned}\right\} \tag{55}$$

Finally, eqs. (53) and (55) together with eqs. (48)−(50) give the solution for eq. (37).

Figure 26 shows a change of deflection pattern of an ice beam with the non-dimensional speed for the damping factor $B=0.1$. The deflection is expressed in the form of w/w_{static}, where w_{static} is the static depression depth. That $B=0.1$ means small damping. It is clear from the figure that the deflection patterns are quite similar to the present experimental results (Fig. 6).

The variation of the depression depth divided by w_{static} is demonstrated for various values of B in Fig. 27. The maximum amplification factor (ratio of the depression depth at u_c to w_{static}) depends on B : an increase in B decreases the maximum amplification factor. In the case of no damping, it becomes infinite.

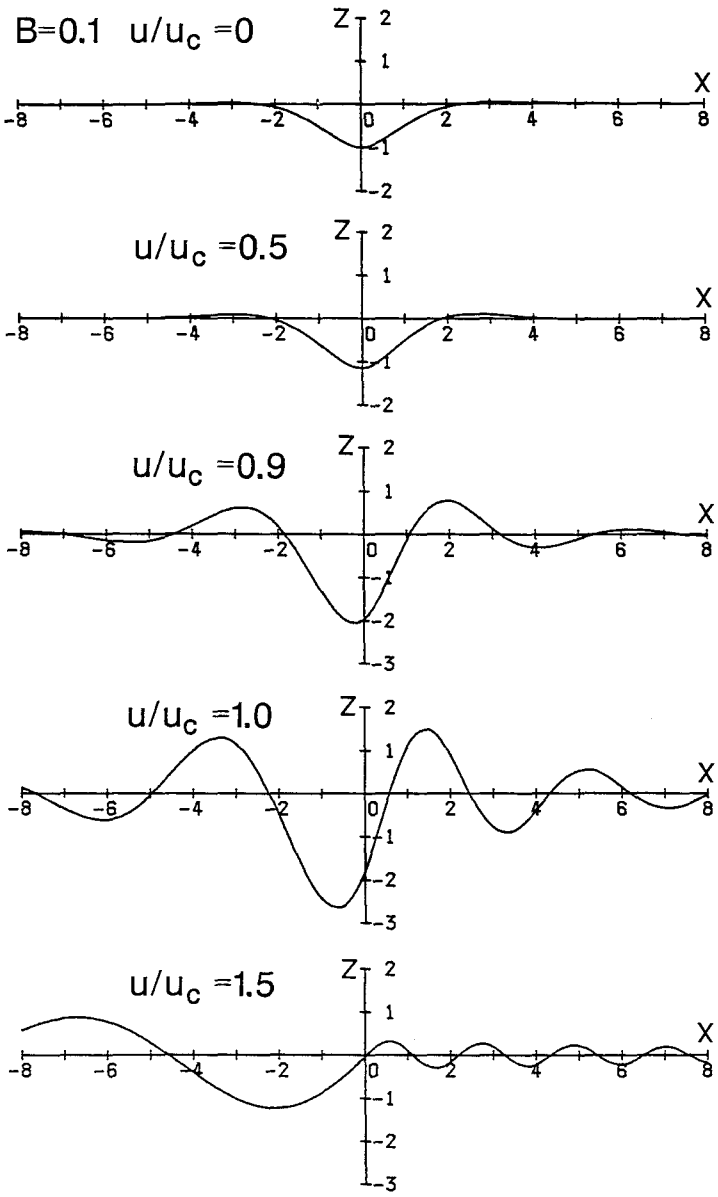

Fig. 26 Deflection patterns of an ice beam for various non-dimensional load speeds u/u_c for damping factor $B=0.1$.

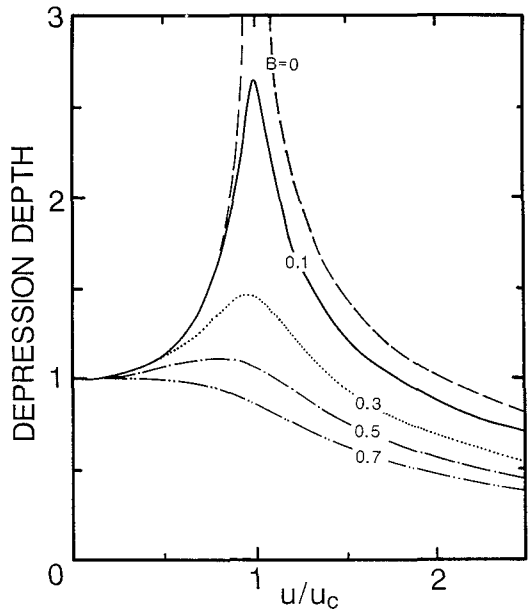

Fig. 27 Non-dimensional plot of the depression depth against the load speed u/u_c for various values of the damping factor B.

Bates and Shapiro (1981) have discussed the response of a floating viscoelastic ice plate to a moving line load. The four parameter model was adopted as a viscoelastic model for ice. The maximum loading factor, which was comparable to the maximum amplification factor, was found to be inversely proportional to the ratio of the elastic modulus of the lead spring to the viscosity of the lead dashpot in the Maxwell unit. The maximum amplification factor or loading factor may serve as an index to the viscoelasticity of ice. As described is Section III.4, the previous experimental values of the maximum amplification factor were approximately 2−4, and young sea ices had large values. The curve for $B=0.1$ in Fig. 27 has the factor of 2.65, which is close to the present experimental value of about 3. Furthermore, its variation agrees fairly well with the experimental result shown in Fig. 9.

From another viewpoint, Schulkes and Sneyd (1986) have discussed theoretically the maximum amplification factor. They treated this as an elastic and time-dependent problem and showed that even without dissipation, the displacement at u_c is limited by the time the load has been traveling. In other words, the present study pointed out that the viscoelasticity of ice specifies the magnitude of the factor ; however, Schulkes and Sneyd found that the ice deflection grows in time as $t^{1/2}$, and the travel time (how long the load travels at the constant speed of u_c before reaching the observation point) determines the factor. The physical explanation of this theory has been given in Section IV.3 : namely, when the load

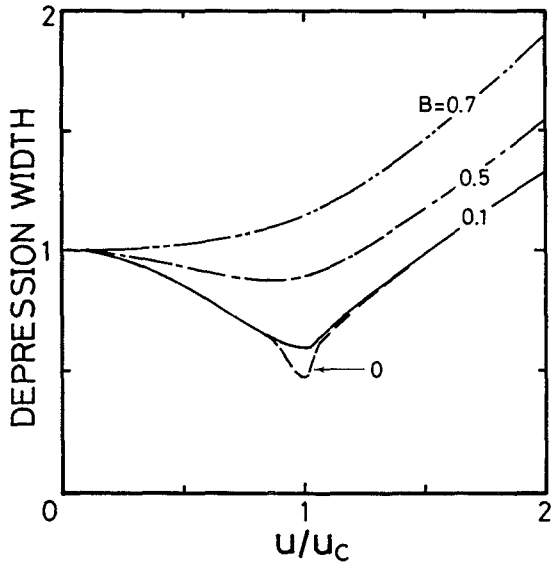

Fig. 28 Non-dimensional plot of depression width against load speed u/u_c for various values of the damping factor B.

moves at u_c, the group velocity is equal to the load speed, so that energy accumulates continuously in the vicinity of the load ; consequently, the ice deflection grows with time. Their result gave the factor of 3.3 for the present experiment, which was comparable to the observed value of about 3. The author has used the skidoo for many years and has frequently driven it at around u_c for several minutes. So far, no growth of ice deflection with time has been found, though there is no experimental evidence to support this point. The above theoretical prediction is interesting, however, and it appears to be worth surveying in field tests.

It is noticeable that the peak position of the curve shifts to the lower speed with increasing B ; this indicates that the critical speed changes with B. When B is small, however, it shifts very little. Hence in the case of small damping such that $B=0.1$, the critical speed is practically the same as that when $B=0$ (no damping).

The variations of the depression width and the lag are shown in Figs. 28 and 29, respectively. Divided by $\sqrt{2}\,N$, both are expressed in the non-dimensional form. The curves for $B=0.1$ resemble the observed variations (Figs. 10 and 11). Particularly, unless the damping effect is taken into account, the change of lag in Fig. 11 cannot be explained, as mentioned earlier in Section III.6.

Thus, it has been revealed that a simple viscous damping model such as eq. (29) is highly applicable to describe the deflection patterns of floating ice sheets, though only in a qualita-

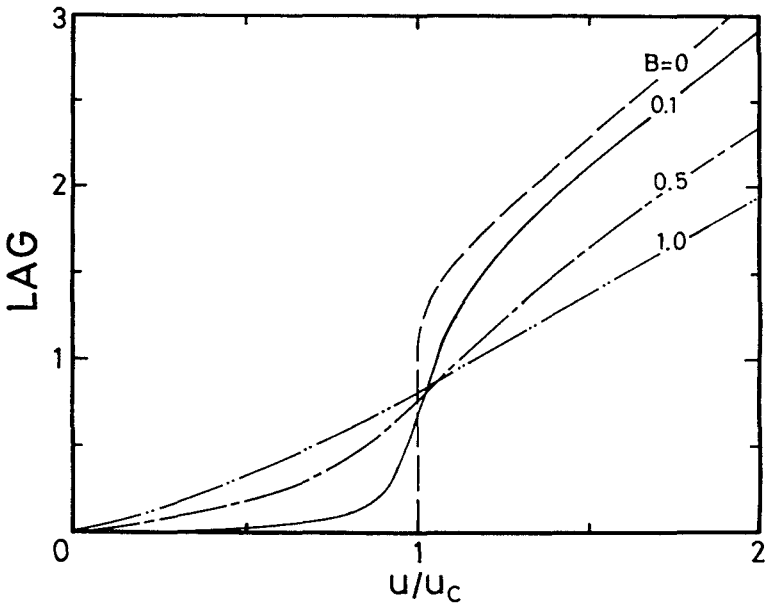

Fig. 29 Non-dimensional plot of the lag against load speed u/u_c for various values of the damping factor B.

tive manner. The good agreement between the solution for $B=0.1$ and the experimental results indicates that small damping is an important factor in the ice response. Furthermore, when viscoelasticity is included in the equation of motion for floating ice sheets such as eq. (3), this simple viscous damping model appears to be adequate to formulate its effects.

It should be noted that in Section IV, the critical speed and the dispersion relation were studied, using the elastic theory ; on the other hand, in this Section, viscous damping was found to have some noticeable effects on the response of the ice to the moving load. In the strict sense, when we discuss the critical speed and the dispersion relation, viscoelasticity must be included. However, there are few differences in the dispersion curve and the critical speed between the cases with no damping and those with small damping. In fact, as already noted, the theoretical curve was able to represent satisfactorily the experimental data (Figs. 14−16). Hence, as far as our purposes are concerned, the elastic theory gives a sufficiently close approximation.

Finally, as another example of the damping effect, we consider here the attenuation of ice waves. Figure 6 showed that the wave amplitude attenuated to zero in about 10 s, even at the beginning of the two-wave stage. The attenuation rate increased with speed. This suggests that the attenuation of the ice wave depends not only on the time but also on the load speed. As mentioned before, the load speed assigns wave characteristics such as frequency

and wavelength. Assuming an exponential wave decay, an amplitude attenuation coefficient for time $\alpha_t(1/s)$ was calculated. Figure 30 is a log-log plot of α_t against frequency f. The power law regression analysis gives

$$\alpha_t = 0.56 f^{0.65}, \tag{56}$$

with a correlation coefficient of 0.84.

The attenuation of ice waves in floating ice sheets has been studied in connection with the penetration of ocean swell into ice covers (e.g., Robin, 1963 ; Wadhams, 1975 ; Wadhams, 1978 ; Squire and Allan, 1980 ; Squire and Moore, 1980 ; Squire, 1984). These studies have disclosed that the attenuation rate increases with wave frequency ; that is, waves with higher frequency are attenuated more rapidly than those with lower frequency. This is consistent with the present result illustrated in Fig. 30. Note that the above authors discussed the attenuation coefficient for distance α_d. Wadhams (1978) found an empirical square relationship between α_d and f : $\alpha_d \propto f^2$. The experimental data by Squire and Moore (1980) agreed with this relationship. On the other hand, the exponent of (56) was 0.65, much smaller than 2. The data points in the higher frequency range, however, seem to be expressed by a square relationship. So far, as suggested by the recent theoretical and

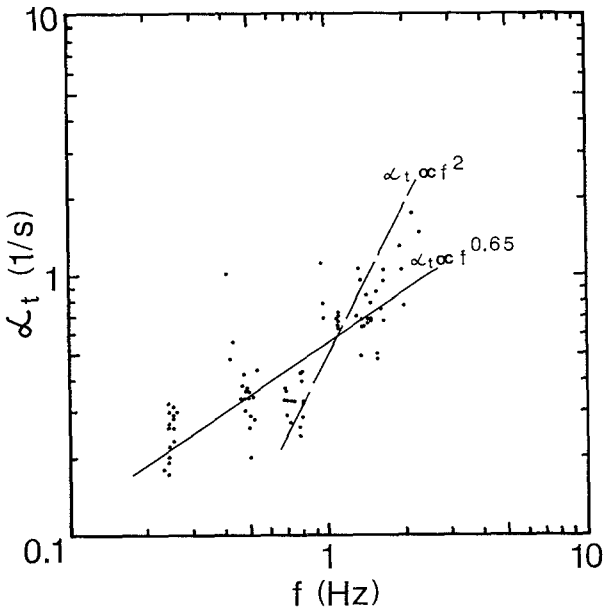

Fig. 30 Attenuation coefficient α_t against frequency f.

experimental work of Squire (1984), there appears to be no simple relation that can adequately describe this problem.

VII. Classification of ice response

In Section III.2, the ice deflection pattern was tentatively divided into five stages. Meanwhile, Eyre (1977) divided it into four modes ; namely, the quasi-static mode ($0<u/u_c<0.7$), the symmetric transition mode ($0.7\leqq u/u_c<0.85$), the asymmetric transition mode ($0.85\leqq u/u_c<1.0$) and the wave-generating mode ($u/u_c\geqq 1.0$). Since Eyre did not observe the trailing wave, he considered only the leading wave in the wave-generating mode. The term "symmetric" means that the load was located in the center of the depression at low speeds in his experiment, so that the deflection profile was symmetrical about the load position. The center of the depression, however, was found to lag behind the load at fairly low speeds (Section III.6 and Fig. 11). Hence, it follows that whether the profile is symmetric or asymmetric is not appropriate in dividing the stages.

Squire *et al.* (1985), on the other hand, divided the load speed into two domains, the sub-critical and the super-critical domains. Corresponding to these domains, the ice response can be called the quasi-static and the wave-generating stages, respectively. Note that they recognized the existence of two waves in the super-critical domain. As they mentioned, there are no theories or experiments which adequately describe the transition stages, except for Eyre's classification. This is because the interest and aims of many studies have centered on the bearing capacity due to static loads, the critical speed and the characteristics of ice waves. The present experimental results showed that the ice deflection pattern changed markedly in the late-transition stage : the depression depth deepened rapidly (Fig. 9) ; the lag increased considerably (Fig. 11) ; and the lag time showed a drastic jump (Fig. 13). These facts suggested that the response nature of the ice to the moving load changed substantially in this stage. Eyre (1977) measured the noises of ice fracture and found their intensity to be maximal at a speed of $0.85u_c$. He designated this speed as the peak-fracture speed u_{pf} and considered it to be more dangerous than u_c. Allowing for experimental error, the value $0.85u_c$ should be regarded as being equivalent to the boundary speed of 5 m/s between the early-transition and the late-transition stages in the present experiment ; in the strict sense, 5 m/s corresponds to $0.86u_c$ (Section III.2). Whether or not u_{pf} is actually dangerous has not yet been verified, but the late-transition stage is a distinctive stage. Therefore, this stage should not be neglected or merely included among the other stages.

The single wave is the typical characteristic of the single-wave stage. In addition to the single wave, however, this stage has the following outstanding characteristics :

(1) The depression depth is smaller than that when $u=0$ m/s (Fig. 9).

(2) The ice beneath the load is not depressed but is somewhat elevated (Fig. 20).

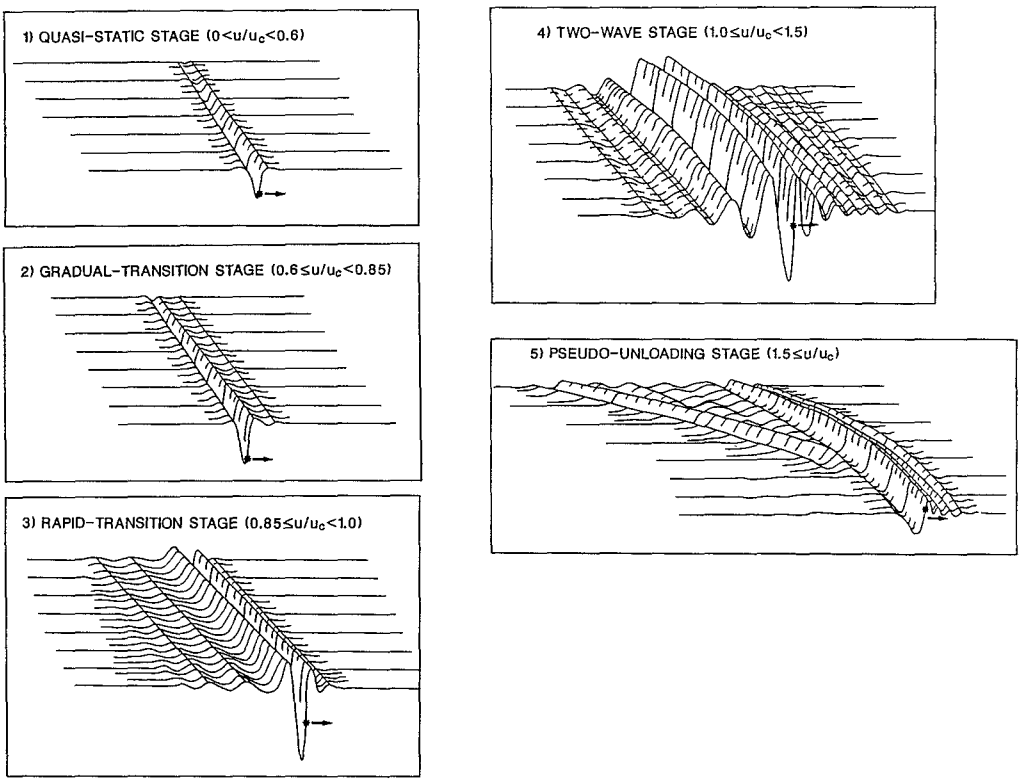

Fig. 31 Schematic images of ice deflection patterns for five stages of ice response.

(3) The shadow zone appears behind the load (Section V.4 and Fig. 23).

As mentioned in Section V.4, the single wave is most likely a virtual state. Hence the term "single-wave" may be inadequate to represent this stage. Regardless of its technical name, this stage is significant and should be distinguished.

Eyre (1977) and Takizawa (1978) pointed out that at faster speeds ($u>2\sim2.5u_c$), the leading wave also disappeared ; that is, only the depression preceded by a somewhat elevated rim was observed. The cause of this phenomenon may be attributed to the decrease of the amplitude of the ice wave below the threshold of detection by the deflectometers.

In conclusion, the present author proposes the following classification (Fig. 31) :

(1) Quasi-static stage : $0<u/u_c<0.6$.
The over-all pattern is similar to the static deflection profile. The center of the depression, however, slightly lags behind the load.

(2) Gradual-transition stage : $0.6\leqq u/u_c<0.85$.

The depression becomes progressively deeper and narrower.

(3) Rapid-transition stage : $0.85 \leqq u/u_c < 1.0$.
The depth deepens rapidly and the lag increases considerably. The lag time shows a drastic jump. (Ice fracture noises have a maximum intensity at $u = 0.85u_c$; (Eyre, 1977))

(4) Two-wave stage : $1.0 \leqq u/u_c < 1.5$.
Two waves are generated. The depression is maximal in depth and minimal in width at u_c. Above u_c, it becomes shallower and wider. The wave amplitude of the rear left and right of the load is larger than that just behind it.

(5) Pseudo-unloading stage : $1.5 \leqq u/u_c$.
The depth is smaller than that at $u = 0$ m/s. The ice beneath the load is not depressed but somewhat elevated. The shadow zone appears behind the load, so that it is likely that an observer standing near the track cannot notice the trailing wave.

VIII. Discussion

VIII. 1 *"Wavelength" at speeds below* u_c

Squire *et al.* (1985) presented some graphs of the wavelength against the speed. Note that the wavelength was derived from ice strain records. They defined "wavelength" (termed "strain wavelength" below) at speeds $u < u_c$ as the distance between two negative peaks around the maximum positive strain. The "strain wavelength" should be compared with the distance between the two peaks of the forward and the backward rims of the depression at the quasi-static to the rapid−transition stages in the present study ; hereafter, this distance is referred to the "deflection wavelength". The "strain wavelength" is, however, smaller than the deflection one. According to Wyman's theory (1950), which gave deflections of floating ice sheets under static loads, the "strain wavelength" is $4.2L$ and the "deflection wavelength" is $9.9L$, when $u = 0$ m/s. Squire *et al.* (1985) showed that the "strain wavelength" was constant at low speeds and that it gradually increased at speeds near u_c. The "deflection wavelength" itself was not obtained in the present experiment, because the rim peaks were often too obscure to be determined. But the depression width is reasonably expected to indicate a similar trend to the "deflection wavelength". Thus, Figure 10 suggests that the "deflection wavelength" decreased with increasing speed in the sub-critical domain. This decrease was due to the shrinkage of the depression profile. This shrinkage necessarily produced the shrinking of the shape of the strain curve corresponding to the depression profile. Presumably, the "strain wavelength" in the present experiment decreased with increasing speed. This speculation, however, is not consistent with the result of Squire *et al.* (1985). Thus this problem should be subjected to future detailed experiments.

VIII. 2 *Effect of in-plane forces*

Kerr (1983) showed that in-plane forces in a floating ice sheet, which are due to a change of thermal conditions in the ice and/or to wind blowing across the ice sheet, have a noticeable effect on the critical speed u_c : when the ice is in tension, u_c is increased, and when in compression, it is decreased. Ono (1976) estimated a constrained stress at 65 kPa by measuring constrained thermal strains in fast ice of 2.1 m thickness at Barrow, Alaska, U.S.A. Assuming that a laterally compressive stress due to wind blowing across a pack ice field is in the range of 0−70 kPa, Bates and Shapiro (1980) evaluated its effect on u_c. When the stress is 70 kPa for 1.5 m thick ice, u_c is reduced by only a few percents at most. Thus, for thick ice, the magnitude of in-plane forces possible under the natural condition may have little effect on u_c.

Meanwhile, as for the thin ice used in the present experiment, Kerr's theory predicts that in-plane forces such as the magnitude of 70 kPa produce a noticeable effect. Applied to the present experimental condition, equation (20), which does not include the effect of in-plane forces, gives $u_c=5.8$ m/s for $L=2$ m. The experimental value of u_c was 5.8 m/s (Section III. 4). It appears, therefore, that there were very little if any in-plane forces, and practically, u_c was not affected by them, though they were not measured in the experimental field. Moreover, on the basis of their experimental results, Squire *et al.* (1985) estimated the forces to be rather small. In addition, Schulkes *et al.* (1986) concluded that these forces are unlikely to have any significant effect. Squire *et al.* (1985) proposed to omit any effects due to in-plane forces with the understanding that this could be a source of error. The present author agrees with this proposal. Undoubtedly these forces are created in ice sheets under the natural condition. Such forces, however, are difficult to quantify in most cases. Hence, considering the conclusions of the studies mentioned above, the omission of the effects due to in-plane forces probably does not introduce significant errors. In addition to instrumental errors, the obtained data include errors due to various factors which are not taken into account such as viscoelasticity and inhomogeneity of ice, except for in-plane forces. It seems acceptable that in-plane forces should be counted among the possible sources of error until their significant effects can be elucidated in field experiments.

VIII. 3 *Characteristics of deflectometers*

The experimental results revealed the existence of two waves, which contradicts the conclusion by Eyre and Hesterman (1976) and Eyre (1977) that a moving load generates only one orderly wave in front of it. This discrepancy may be caused by a difference in instrumentation. The conventional bottom-anchored deflectometer used in the present experiment is so insensitive to high-frequency ice oscillations that it responds only to the primary mode of ice motion. Furthermore, it gives a direct reading of ice deflection. On the other hand, the deflectometer used by the above authors is a sensitive water pressure transducer.

The responses measured by their deflectometer include hydrodynamic pressure disturbances in addition to purely hydrostatic effects that reflect ice deflection. The high-frequency fluctuations due to pressure disturbances are expected to increase, particularly in the load's wake. Consequently, they appear to obscure the primary response to the trailing wave.

IX. Concluding remarks

On the basis of the field experimental results, the response of a floating sea ice sheet to a steadily moving load has been discussed in this study. The major results are as follows :

(1) The existence of two ice waves was confirmed.
(2) A diagram that predicts the critical speed was presented.
(3) The spatial nature of the ice deflection pattern was clarified.
(4) The viscoelasticity of ice was found to have some significant effects on the ice response.
(5) Classification of the ice response into five stages was proposed.

Acknowledgements

The author wishes to express his gratitude to the late Professor T. Tabata and Professor emeritus of Hokkaido University, Z. Yoshida, for their guidance and encouragement. He is also much indebted to Professors N. Ono, Y. Suzuki and T. Kuroda and Dr. M .Wakatsuchi of the Institute of Low Temperature Science, Dr. T. Sasatani of the Faculty of Science and Dr. M. Nakawo of the Faculty of Engineering, Hokkaido University, for their valuable discussions and helpful comments. He is also grateful to Professor M. Aota, Dr. T. Kawamura, Messrs. M. Oi, M. Ishikawa and H. Fukushi of the Sea Ice Research Laboratory of Hokkaido University for their kindness in offering logistic support and help in the field experiments. Special thanks are extended to Messrs. M. Oi and H. Fukushi for their technical skill and enthusiasm in making the skidoo detectors and the computer program used for data processing. The field experiments could not have been performed without the assistance of Drs. K. Shirasawa and Y. Nohguchi, and Messrs. T. Saito, S. Kohno and T. Motoi. The author acknowledges the technical support and encouragement of the above persons for the valuable part they played in this investigation. Figure 23 is reproduced from Davys, J. W., Hosking, R. J. and Sneyd, A. D. in J. Fluid Mech., vol. 158, 269–287, 1985, by permission. Acknowledgement is due to the authors above and the editor.

References

Bates, H. F. and Shapiro, L. H. 1980 Long-period gravity waves in ice-covered sea. *J. Geophys. Res.*, **85**(C2), 1095–1100.

Bates, H. F. and Shapiro, L. H. 1981 Stress amplification under a moving load on floating ice. *J. Geophys. Res.*, **86**(C7), 6638–6642.

Beltaos, S. 1979 Field studies on the response of floating ice sheets to moving loads. Proc. Workshop on the Bearing Capacity of Ice Covers, 16–17 October 1978, Winnipeg, National Research Council of Canada, Technical Memorandum No. 123, 1–13.

Davys, J. W., Hosking,R. J. and Sneyd, A. D. 1985 Waves due to a steadily moving source on a floating ice plate. *J. Fluid Mech.*, **158**, 269–287.

Eyre, D. and Hesterman, L. 1976 Report on an ice crossing at Riverhurst during the winter of 1974–1975. Report No. E76–9, Saskatchewan Research Council, Canada.

Eyre, D. 1977 The flexural motions of a floating ice sheet induced by moving vehicles. *J.Glaciol.*, **19**(81), 555–570.

Hertz, H. 1884 Über das Gleichgewicht schwimmender elastischer Platten. *Wiedemann's Ann. Phys. Chem.*, **22**, 449–455.

Kerr, A. D. 1976 The bearing capacity of floating ice plates subjected to static or quasi-static loads. *J. Glaciol.*, **17**(76), 229–268.

Kerr, A. D. 1983 The critical velocities of a load moving on a floating ice plate that is subjected to in-plane forces. *Cold Reg. Sci. Tech.*, **6**(3), 267–274.

Kubo, Y. 1958a Loading capacity of ice-plate (1). *Seppyo*, **20**(3), 75–78 (in Japanese).

Kubo, Y. 1958b Loading capacity of ice-plate (2). *Seppyo*, **20**(4), 97–104 (in Japanese).

Lighthill, J. 1978 Waves in fluids. 1st ed., Ch.4, Cambridge University Press, Cambridge, UK.

Nevel, D. E. 1970 Moving loads on a floating ice sheet. Research Report 261, U.S. Cold Regions Research and Engineering Laboratory.

Ono, N. 1976 Arctic sea ice research. III. Measurements of state of thermal stress induced in surface layer of sea ice cover. *Low. Temp. Sci., Ser.* **A, 34**, 221–226 (in Japanese).

Robin, G. de Q. 1963 Wave propagation through fields of pack ice. *Phil. Trans. Roy. Soc. London, Ser.* **A, 255**, 313–339.

Schulkes, R. M. S. M., Hosking, R. J. and Sneyd, A. D. 1986 Waves due to a steadily-moving source on a floating ice plate II. Mathematics Research Report No. 147, University of Waikato, New Zealand.

Schulkes, R. M. S. M. and Sneyd, A. D. 1986 Time-dependent response of floating ice to a steadily -moving load. Mathematics Research Report No.149, University of Waikato, New Zealand.

South Manchurian Railway Company. 1941 Kahyō tokuni hyōjōkidō ni kansuru kenkyū [Studies on river ice ; with special reference to the construction of railroad on ice] (in Japanese).

Squire, V. A. and Allan, A. J. 1980 Propagation of flexural gravity waves in sea ice. In Sea Ice Processes and Models (R. S. Pritchard *ed.*), University of Washington Press, Seattle, U.S.A., 327–338.

Squire, V. A. and Moore, S. C. 1980 Direct measurement of the attenuation of ocean waves by pack ice. *Nature*, **283**(5745), 365–368.

Squire, V. A. 1984 A theoretical, laboratory and field study of ice-coupled waves. *J. Geophys. Res.*, **89**(C5), 8069–8079.

Squire, V. A., Robinson, W. H., Haskell, T. G. and Moore, S. C. 1985 Dynamic strain response of lake and sea ice to moving loads. *Cold Reg. Sci. Tech.*, **11**(2), 123–139.

Tabata, T. 1959 Studies on mechanical properties of sea ice. IV. Measurement of internal friction.

Low. Temp. Sci., Ser. **A, 18**, 131−148 (in Japanese).
Takizawa, T. 1978 Deflection of a floating ice sheet subjected to a moving load. II. *Low Temp. Sci., Ser.* **A, 37**, 69−78 (in Japanese).
Takizawa, T. 1985 Deflection of a floating sea ice sheet induced by a moving load. *Cold Reg. Sci. Tech.*, **11**(2), 171− 180.
Wadhams, P. 1975 Airborne laser profiling of swell in an open ice field. *J. Geophys. Res.*, **80**(33), 4520−4528.
Wadhams, P. 1978 Wave decay in the marginal ice zone measured from a submarine. *Deep-sea Res.*, **25**, 23−40.
Weeks, W. F. and Assur, A. 1967 The mechanical properties of sea ice. CRREL Monograph II−C3, U.S. Cold Regions Research and Engineering Laboratory.
Wilson, J. T. 1958 Moving loads on floating ice sheets. University of Michigan Research Institute (UMRI Project 2432).
Wyman, M. 1950 Deflections of an infinite plate. *Can. J. Res., Sec.* **A, 28**, 293−302.